BUCKLING BEHAVIOR OF DENTED SHORT CYLINDRICAL SHELLS

Ali AGHAZADEH DIZAJI

M. Sc. Thesis
Department of Civil Engineering
Prof. Dr. Abdulkadir Cüneyt AYDIN
2018

UNIVERSITY OF ATATURK
GRADUATE SCHOOL OF
NATURAL AND APPLIED SCIENCES

M. Sc. THESIS

BUCKLING BEHAVIOR OF DENTED SHORT CYLINDRICAL SHELLS

Ali AGHAZADEH DIZAJI

DEPARTMENT OF CIVIL ENGINEERING

ERZURUM
2018

T.C.
ATATÜRK ÜNİVERSİTESİ
FEN BİLİMLERİ ENSTİTÜSÜ

TEZ ONAY FORMU

BUCKLING BEHAVIOR OF DENTED SHORT CYLINDRICAL SHELLS

Prof. Dr. Abdulkadir Cüneyt AYDIN danışmanlığında, Ali Aghazadeh DIZAJI tarafından hazırlanan bu çalışma 12/06/2018 tarihinde aşağıdaki jüri tarafından İnşaat Mühendisliği Anabilim Dalı'nda Yüksek Lisans tezi olarak **oybirliği/~~oy çokluğu~~ (3/3)** ile kabul edilmiştir.

Başkan : Prof. Dr. Abdulkadir Cüneyt AYDIN *İmza :*

Üye : Prof. Dr. Abdulkadir KAN *İmza :*

Üye : Dr. Öğretim Üyesi Merve SAĞIROĞLU *İmza :*

Yukarıdaki sonuç;

Enstitü Yönetim Kurulu 21.../06.../2018 tarih ve ..25./..34..... nolu kararı ile onaylanmıştır.

Prof. Dr. Mehmet KARAKAN V.
Enstitü Müdürü

Not: Bu tezde kullanılan özgün ve başka kaynaklardan yapılan bildirişlerin, çizelge, şekil ve fotoğrafların kaynak olarak kullanımı, 5846 sayılı Fikir ve Sanat Eserleri Kanunundaki hükümlere tabidir.

ÖZET

Yüksek Lisans Tezi

KISA DENTLİ KABUK TANKLARDA BURULMA DAVRANIŞI

Ali AGHAZADEH DIZAJI

Atatürk Üniversitesi
Fen Bilimleri Enstitüsü
İnşaat Mühendisliği Anabilim Dalı
Yapı Bilim Dalı

Danışman: Prof. Dr. Abdulkadir Cüneyt AYDIN

Silindirik tanklar birçok önemli yapılarda kullanılmaktadır. Bu rezervuarlar genellikle dışarıdan gelen hidrostatik kuvvetlere veya sıvıların boşaltılması sırasında dâhili bir vakuma maruz kalmaktadır. Hidrostatik bir kuvvetin veya dâhili bir vakumun etkisi altında silindirik rezervuarlar üzerinde önemli araştırmalar yapılmıştır. Son yirmi yıl içinde tek tip hidrostatik yükleme ve tek eksenli yükleme altında silindirik ve konik rezervuarlar incelenmiştir. Halka, enine ve boyuna berkitmeler olarak iki ana faktör burkulma yükü için değerlendirilmiştir. Silindirik veya konik kabukların kabuk kalınlıkları yerel (lokal) ve kararlılık bağlamında test edildi.

Bu çalışmada, göçük diş derinliği (tc ve 2tc), ve diş uzunluğu (h/3 ve h/2) kısa silindirik kabuklar için incelenmiştir. İncelenen on silindirin yarıçapı, yüksekliği ve kalınlığı sırasıyla 500 mm ve 1 mm'dir. Karbon fiber takviyesinin (CFRP) etkisini araştırmak için modeller iki gruba ayrılmıştır. CFRP etkisi, CFRP boyutlarının, diş özelliklerine göre tasarlanmasıyla test edilmiştir. Ayrıca, CFRP ile ve CFRP'siz iki kusursuz örnek karşılaştırma için test edilmiştir.

Deneysel karşılaştırmalar, başlangıç ve genel burkulma için teorik formüller kullanılarak değerlendirilmiştir. Bu burkulma esaslı teoriden elde edilen burkulma dalgaları değerlendirilmiş ve tersine dönme yöntemi tarif edilmiştir. CFRP'siz numunelerin çökme yükleri, ilk burkulma yükünün 2,5 katı kadar oluşmuştur. Bununla birlikte, CFRP kullanılan numunelerde göçme burkulması yükünün ve başlangıç burkulması yüküne oranı yaklaşık 1,5 olarak elde edilmiştir. Bu nedenle, CFRP etkisi, deneysel ve teorik modeller için yük şekil değiştirme, yük-yer değiştirme, dalga şekilleri ve dalga sayıları kullanılarak değerlendirilmiştir.

2018, 73 sayfa

Anahtar Kelimeler: Silindirik tank, Göçük, CFRP

ABSTRACT

Master Thesis

BUCKLING BEHAVIOR OF DENTED SHORT CYLINDRICAL SHELLS

Ali AGHAZADEH DIZAJI

Atatürk University
Graduate School of Natural and Applied Sciences
Department of Civil Engineering

Supervisor: Prof. Dr. Abdulkadir Cüneyt AYDIN

Cylindrical tanks are used in many important structures. These reservoirs are often subjected to hydrostatic forces from outside or an internal vacuum during the discharge of liquids. Considerable research has been conducted on cylindrical reservoirs under the influence of a hydrostatic force or an internal vacuum. Cylindrical and cone reservoirs under uniform hydrostatic loading and uniaxial loading were investigated within the last two decades. The two main factors as ring stiffeners and stringers were evaluated for the buckling load and the shell thickness of cylindrical or conical shells were tested for imbalance and localized datum.

Within this work, the dents are investigated for the varying dent depths (tc and 2tc), dent lengths (h/3 and h/2) for short cylindrical shells. The radius, the height and the thickness of the ten cylinders were 500 mm and 1 mm, respectively. The samples are divided to two groups to investigate the effect of carbon fiber reinforcement (CFRP). The CFRP effect is tested by designing the CFRP dimensions according to dent properties. Moreover, two perfect samples with CFRP and without CFRP were tested for comparison.

The experimental comparisary are expended by using theoretical formulas for initial and overall buckling. The buckling waves obtained from the buccaneering theory are evaluated and reversal method described. The collapse loads of the samples without CFRP but dents, are 2,5 times then the initial buckling load. However, the CFRP used samples, the collapse load to initial buckling load ratio was about 1,5. Thus, the CFRP effect is evaluated for the experimental and theoretical models, by using load-strain, load displacement, wave forms and wave counts.

2018, 73 pages

Keywords: Cylindrical tank, Dent, CFRP

ACKNOWLEDGEMENTS

I would like to express my profound appreciation to my devoted and patient supervisor, Prof. Dr. Abdulkadir Cüneyt AYDIN not only for his educational and technical advices throughout this study, but also for all his motivating guidance and discussions to follow the road of life as a follower of reality. I am grateful to be a colleague of him.

I would like to thank my dear friends Dr. Mahmut KILIÇ and Dr. Mahyar MAALI for their valuable helps in various stage of this study.

Finally, thanks to my family and I hope them to continue their way.

Ali Aghazadeh DIZAJI
May, 2018

CONTENTS

LIST OF FIGURES

LIST OF TABLES

1. INTRODUCTION

Thin-walled shell structures are characterized by a lightweight structural form with high strength. This structure has many applications in various engineering fields and is considered to be a basic tool in modern industry. The importance of using cylinders and cone shells has long been known to engineers and designers in various engineering branches. These structures are used in offshore platforms, oil and gas tanks, chimneys, silos and tanks, cooling towers, bodies of ships, submarines, planes, arc dams, missiles and structures are widely used in shell form.

Some of the most important issues are thin-walls in the shell, the manufacturing process, and how the components are assembled. Owing to the low thickness of the walls of the shell structures, it is possible for deformations and disturbances on the wall surfaces to occur. Generally, tanks and silos use smaller and smaller multiple panels, which exhibit geometrical defects in the boiling process.

One of the most important issues to be considered in the investigation of thin-walled steel shells is the effect of geometric imperfections owing to the welding process and the assembly of the component parts of the shells. Tanks, silos, and most large steel-shell structures connect smaller pieces together during the welding process, which causes several types of malformations on the shell walls.

Owing to the longitudinal (peripheral) wiring of the panels, collateral imperfections occur. With transverse waves (meridian), longitudinal imperfections also occur. These types of defects are present in almost all thin shells and are unavoidable to a great extent. The study of the effects of annular and longitudinal imperfections on the bearing capacities and buckling behaviors of shell structures is important. Buckling behavior is related to critical load capacity and structural fractional behavior, after passing the load from the critical stage to failure. Buckling in a cylindrical shell depends on a variety of factors:

1. Geometric properties; radius, height, thickness
2. Properties of materials; including isotropic, composite, and corrugated
3. Loads applied on the cylinder; which include axial, hydrostatic, uniform, torsional, or compound pressures.

A change in any of the above parameters in the cylindrical shell causes a change in the buckling behavior of the shell. The critical load capacity of shells under load depends on the slenderness ratios owing to the effects of length, radius, and thickness. Owing to the remarkable changes in the shell geometry at the moment of buckling, it is necessary to determine the fractional behavior until the complete failure phase. In addition, the initial geometrical defects are very influential in the critical load capacity of the buckling shells. There have been significant studies in this area. These failures can result from manufacturing, assembly, welding, and other processes.

The main objectives of this research are as follows:

1. Investigate the effect of different longitudinal dent sizes and numbers on the buckling and post-buckling capacity, load-radial displacement, and buckling wave forms in the laboratory
2. Provide feedback points related to the inadequate analysis of reservoir design
3. Evaluate the actual behavior of cylinderic shells in the pre-buckling and buckling stages
4. Compare the laboratory results with the theoretical formulations

The importance and necessary of the thesis is presented in the first chapter.

The second chapter, begin with, the concepts of structural instability, methods for studying the phenomena of structural systems and their criteria, and the division of instability phenomena are presented. Finally, a definition of the stability equations of cylindrical girder shells is presented. Moreover, the geometric failures, their types, impact

on buckling capacities, and the history of research on conical and cylindrical shells of thin-walled structures with geometric imperfections are presented and examined.

The third chapter of this thesis deals with laboratory samples, methods of their construction, and the tools and equipment used in experiments.

In the fourth chapter, describes the process of performing each of the experiments in detail, and then provide graphs and drawings obtained from these experiments. In the last section of this chapter, a comparison is made between the results of these experiments, and the results of these comparisons are presented as preliminary laboratory results. At the end of this chapter, a section is devoted to a comparison and conclusion in which the results, laboratory images, theoretical formula, and regulations are compared, and the precision of each is determined.

The fifth and the last final chapter of this thesis deals with the results from the preceding chapters and summarizes their results. At the end of this chapter, a section is also presented as recommendations for future research.

2. LITERATURE REVIEW and BACKGROUND

Considering that the use of thin-walled shells is expanding every day. It is important to examine the problem of instability in this form of structure. Many steel structures such as high water tanks, water and oil reservoirs, marine structures, and pressure vessels, including shell elements, are under stress tension. In addition, shell elements are subject to instability owing to the loads applied. The theoretical buckling resistance (theoretical) is based on a two-branch elastic linear analysis that is suitable for conventional shell cylinder shells. Simple formulas are prescribed for many geometric properties and types of loads (Miller 1999).

2.1. Definitions of Thin-Walled Shells

2.1.1. Mechanical view

From a mechanical point of view, the shells are structures made of shell-bearing elements. In engineering, reducing the structural weight by maintaining a certain resistance is always attempted. Thus, in addition to being economically feasible, the structures will be able to increase lateral forces. One of the common ways to increase strength without weight gain in metal and nonmetallic structures is the use of thin-shell structures. Therefore, thin-walled shell structures have important properties owing to their structure and light weight with high strength.

2.1.2. Geometric view

A shell can be defined as a solid body enclosed between two curved surfaces. The distance between the two pages is as thick as the shell. Therefore, geometric shell structures are surfaces that separate a volume of space from the rest (Mahdi *et al.* 2002). Shell structures have a curved shape, and their thickness is much smaller than the other two dimensions. In some cases, the thickness ratio reaches a radius of 1/3000. Unlike plates, skins, owing

to the curved shape, in addition to the forces and moments available, have the ability to create force on the plate for initial resistance action. The field of forces created in these structures are in the forms of membrane and flexural forces. Depending on the thickness of the shell crest, the flexural forces are variable (Showkati and Ansourian 1995).

2.2. Examining Causes of Structural Instability

The study of stability and instability in thin-walled sections is important for two reasons. First, the thickness ratio to other dimensions in such structures is very low. The same feature highlights instability in them. In addition, shell structures are subjected to forces that create tensile stresses. Therefore, the thinness of the shell on one side, and the pressure of the field of forces on the other, expose the shell to buckling. This, of course, does not mean that shell structures are weaker than other buccal considerations or other structural forms because most of these structures have ultra-strong resistance. In other words, some thin-walled shells still have additional load bearing after buckling (Timoshenko and Gere 1961).

Of course, the fractional capacity, in addition to the geometry, depends more on the type of load involved. Thus, given the application of the crust in the industry, it is essential for engineers to have a practical knowledge of their behavior. The concepts of stability and instability are used with different concepts in different situations. The general concept of sustainability is used in some situations and in situations that usually occur suddenly. From some perspectives, it is somewhat unexpected and it has poor results (Farshad 1994).

To investigate the phenomenon of instability in shell structures, there are a variety of methods that are important in terms of their application scope. First, scientists put forward a number of theoretical and theoretical questions about the implications of shell instability, and resolved the sustainability of these structures under different loadings, but these methods were often based on simple assumptions. For complex shell problems, the solutions of differential equations are impossible except in special cases. In addition to

theoretical considerations, conducting lab tests on real-world samples is the most documented and most cost-effective approach. However, one of the issues that should be considered in laboratory techniques is that there is no possibility of constructing geometric impediments. This causes differences between theoretical and laboratory results.

With the advent of numerical methods, a great transformation emerged in solving differential equations. It is worth noting that owing to the smooth uniformity and simple geometry of rotating shells, the study of the behavioral stability of this type of structure is the basis and a good reference for comparison with more complex modes, as well as shells in general. In addition, the governing equations in the stability of thin-walled shells are simpler than those of shell-shell equations. It is easier to study shells as a prelude to the more complicated problem of shell stability (Brush and Almorth 1975).

Many examples of stability and instability can be found in chemical reactions, air flow, river flow, and the human body state. There are many examples in which the structures are interrupted by the instability of their equilibrium. These samples include construction frames and their elements, bridges, silos, cooling towers, marine structures, and pipelines. In structural frames, lean compression members undergo relatively high load losses (Chen and Lui 1987).

The fundamental method of interpreting the sustainability of a reactionary system is to use the concept of energy as the minimum total potential. In nature, an elastic system always tends to be in a state where the energy of the total potential is minimal. A system of time is in a stable equilibrium where any deviation from its initial state of equilibrium results in an increase in the total potential energy of the system. In an unstable system, any deviation from the initial state of equilibrium results in a decrease in the total potential energy of the system.

Finally, there is a neutral equilibrium system in which any deviation from its initial state of equilibrium results in an increase or decrease in the total potential energy. Owing to

this principle, the concept of energy can be used to find the critical load of a reactionary system (Chen and Lui 1987).

2.3. Investigation of Instability Analysis of Structural System

The concept of sustainability can be used to determine the critical condition of a reactive system that is susceptible to instability. Methods of investigation of structural instability phenomena include:

- Static approach
- Energy approach
- Dynamic approach

2.3.1. Static approach

In a static method, a state in which there are two or more different but close-to-balance modes can be followed by analyzing a special geometric amount. Using the least amount of time with this mode is critical. The static method is also known as the special amount method because the techniques used in this method are the same as the technique used to determine the specific value of a matrix. Critical conditions are shown with special values of the system hardness matrix, and the spatial states are obtained with special vectors. The least special value is the critical load of the system. This method is an approximate mathematical method for determining the critical condition of a system without inequality (Chen and Lui 1987).

2.3.2. Energy approach

The energy method is a practical way to calculate the approximate critical load. This approach was provided by Tymoshenko. For an elastic system exposed to sustained loads, the total potential energy of the system can be expressed as a function of the set of general

displacement and external forces. If the system is in equilibrium, its total potential energy must be constant. Therefore, by putting the first derivative of the total energy function (the sum of the energy of the elastic strain and the potential of the external forces) in terms of any total displacement of zero, we can determine the system equilibrium conditions and calculate the critical load from the equilibrium equations (Chen and Lui 1987).

2.3.3. Dynamic approach

A system of motion equations in which the vibration of a small free space dominates the system is written as a function of public change and external forces. When the movement is limited, the critical load is obtained as a balance of external forces. If a small disturbance causes the system to deviate from the initial position, the equilibrium is stable, and if the magnitude of the turbulence decreases, the magnitude of the deviation decreases. If the magnitude of the motion increases without limit, then the equilibrium is unstable when exposed to small disturbances (Chen and Lui 1987). This method is used to calculate the critical load of an elastic system.

2.4. Types of Unstable Phenomena

The stability of a structural system depends on structural parameters such as geometric properties, materials, and environmental conditions such as loading conditions. Sustainability phenomena can be classified as follows: Doppler dot instability, terrain point instability, and dynamic and vibrational instability.

2.4.1. Bifurcation point

One of the common types of static elastic instability is the bipartite equilibrium state. This type of instability is based on the fact that a member or system that initially changes in the direction of applied loads suddenly changes in the other direction. The transitional point of the usual mode, called deformation to a variable mode, is deformation to the point of equilibrium. The load on the equilibrium point is called the critical load. The

deformation pathway, which is preceded by a two-branch location, is called the primary or basic pathway and the deformation path after the second branch of the secondary path. The secondary path shows the stability regime, and the first path is unstable at the point of two branches (Fig. 2.1). From a physical point of view, the system chooses a path that meets the minimum of its potential energy (Farshad 1994).

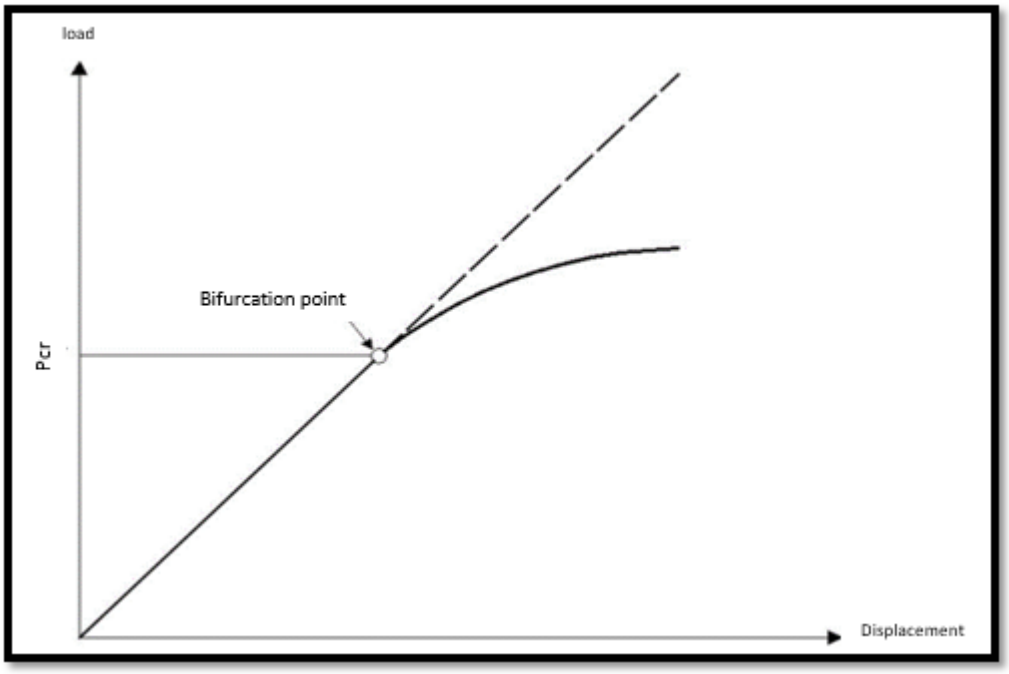

Figure 2.1. Two-branch equilibrium overview (Farshad 1994)

Depending on their nature, the secondary paths of buckling (two types of instability in the region of two branches) can be defined as two symmetric branches or two asymmetrical branches.

In symmetric two-branch mode, the buckling paths are symmetric if the post-buckling paths, after the critical load is ascending, are said to provide a stable symmetric two-branch system. In such a system, the load required to maintain buckling stability increases with increasing radial change [Figure 2.2 (a)]. If post-buckling paths are downstream after a critical load, then the system is said to be symmetric and unstable. Such a system, which

is required to maintain stability after buckling, the load decreases with increasing displacement [Figure 2.2 (b)].

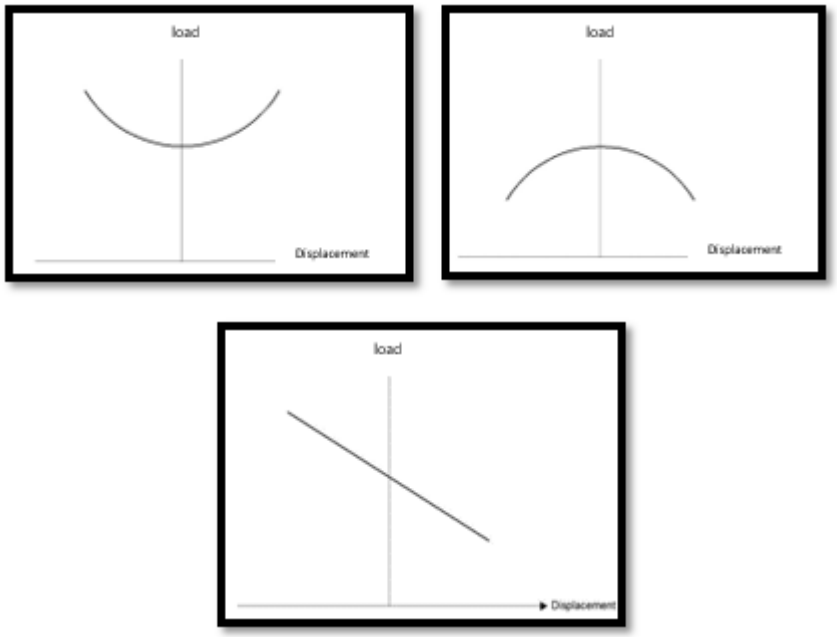

Figure 2.2. Post-buccal behavior in bipartite state
(a) symmetrically stable, (b) symmetrically unstable, and (c) asymmetric.

In an asymmetric biphopatic mode, the load required to maintain buckling stability may increase or decrease with increasing displacement depending on the direction in which the structure changes after buckling. In Figure 2.2 (c), the asymmetric bipartite behavior of the system is shown schematically.

2.4.2. Point-to-point instability

The point-of-point instability, as can be understood implicitly in its naming, is referred to as instability, which occurs at the maximum point in the load-shift curve. At this point, the maximum limit of equilibrium is observed at the end of the initial path. The lack of stability results from limitations of stability in structures that tolerate transverse loading more than axial compression loading (Chen and Lui 1987). In this type of sustainability, there is only one deformation mode: from the start of loading to the maximum load. In

this type of instability, a buckling of the intersection will be seen owing to the presence of a nonlinear path.

2.4.3. Dynamic and vibrational instability

Instability is caused by the dynamic and volatile effects of so-called vibration. Both dynamic instabilities are such that motion and equilibrium are dynamically unstable. Dynamic instability means that an unstable system has fluctuations with increasing ranges. Structures exposed to time-dependent forces and sudden loading are dynamically unstable for a short period of time. For example, a column under a shock-absorbing force loses its steady state under a dynamic regimen.

In addition, the stability state of an elastic system under static forces may be unstable in a dynamic fashion. For example, a static structure under a nonpermanent force tolerates fluctuations with increasing amplitudes. This instability is called vibrational instability. Infinite vibrations of bridges under wind loads, vibrations of space ships during their uniform motion, and vibration of liquid transmission pipes are examples of vibrational instabilities (Chen and Lui 1987).

2.5. Study of Stability Equations of Thin-Walled Cylinder Shells

The study of shell structures and their stability is important. The history of applying stability equations to shell structures dates back to ancient times. In 1795, Euler established the theory of stability of beams (Mazurkiewicz and Nagorski 1991). Then, the theory of the problems of shell-structure mechanics and many methods of solving them was introduced, and a large number of researchers have since dealt extensively with this subject. A general theory of shells was presented for the first time in the second half of the nineteenth century by Love (1959).

Experimental tests are evaluated to observe the initial buckling load of cylindrical shells. Then, these results are compared with the relevant codes and standards per Jawad (1994),

Venstel and Krauthaer (2001), Ross (2007), the British Standards Institution Code (2009), and the European Recommendations Code (1988).

Jawad (1994), Venstel and Krauthaer (2001), and Ross (2007) obtained the critical load of the external pressure (P_{cr}) in cylindrical shells. Cylindrical shells are assumed to be simply supported with axial restraints in these equations:

Jawad theory: $P_{cr}= \frac{0.92\, E(\frac{te}{R})^{2.5}}{\frac{Le}{R}}$

Venstel and Krauthaer theory: $P_{cr}= 0.92\, \frac{Et}{L}(\frac{t}{rm})^{1.5}$

Ross theory: $P_{cr} = \frac{2.6E(\frac{t}{d})^{2.5}}{\frac{H}{d} - 0.45(\frac{t}{d})^{0.5}}$

In these theories, E = Young's modulus = modulus of elasticity, R = radius of the cylindrical shell, rm = mean value of the radius, t = te = effective thickness, d = mean diameter of the cylindrical shell, and Le = H = length of the cylindrical shell.

The British Standards Institution code (BSI) (2009) in the fourth edition of the Specification for Unfired Fusion Welded Pressure Vessels is also considered in this study. The code predicts the elastic instability pressure (P_{mc}) for shell structures. In this theory, ε is a parameter that is a function of 2Rm/t and L/2Rm. Rm is the radius of the cylindrical shell.

British Standards Institution code (BSI) theory: $P_{mc}=\frac{Et\varepsilon}{R_m}$

Last, the design formula provided by the European Recommendations ECCS-CECM-EKS for the Buckling of Steel Shells (ECCS, 1988) is considered in this research and is used to predict the buckling pressure of simply supported elastic shell structures. In this

formula, βmin is a parameter that is a function of t/re and L/re, where re is the radius of the cylindrical shell:

European Recommendations code (ECCS) theory: $Pcr = E\frac{t}{re}\beta min$

The theoretical predictions of Jawad, Venstel and Krauthaer, Ross, the British Standards Institution Code, and the European Recommendations Code for the initial buckling pressure of a perfect model is summarized in section 4. The number of circumferential buckling waves is calculated through approximations by Fatemi *et al.* (2013) and Teng *et al.* (2001):

$$n = 2.74\sqrt{\frac{R}{L}\sqrt{\frac{R}{t}}}$$

Where t is the thickness, R is the radius, and L is the height of the cylindrical shell. The number of circumferential buckling wave's theory given that section four. Thus, the results of the above relations will be used to evaluate and validate the results of the analysis in this thesis.

2.6. Background of Thin-walled Shells

There are many research studies about thin-walled structures. Teng and Hu (2007) examined the benefits of FRP confinement of hollow steel tubes. Axial compression tests on FRP-confined steel tubes were first described. The finite element modeling of these tests was then discussed. Both the tests and numerical results indicated that FRP jacketing is a very promising technique for the retrofitting and strengthening of circular hollow steel tubes. In addition, finite element results for FRP-jacketed thin cylindrical shells under combined axial compression and internal pressure were presented to show that FRP jacketing is also an effective strengthening method for such shells when a fail occurs by elephant's foot collapse near the base. The failure modes of Teng and Hu's 2007 experimental tests are shown in Figure 2.3.

Figure 2.3. Collapse modes in research by Teng and Hu (2007).

Batikha *et al.* (2009) investigated a novel method of strengthening cylindrical shells against elephant's-foot buckling in which a small amount of FRP composite used at a critical location can effectively eliminate the problem and increase the buckling strength. The strengthened shell was analyzed using linear elastic bending theory in this preliminary study. Within the scope of this research, the strengthening effect was shown to be sensitive to the thickness, height, and location of the FRP sheet. The issue of optimal FRP strengthening to allow the shell to attain puremembrane-state deformation was examined in detail, as strengthening with too much and too little FRP are both undesirable. Both pinned-based and fixed-based shells were examined, and their responses were compared.

Maali *et al.* (2012) discussed 14 laboratory specimens in two groups: Shallow Conical Caps (SCC) and Deep Conical Caps (DCC). These were loaded under uniform hydrostatic pressure. The samples were modified to include either one or two line imperfections with amplitudes of 1t, 2t, and 3t in depth (t is the thickness of the conical shell). The results

presented here are in general agreement with international codes as well as theories concerning initial and overall buckling and collapse. Generally speaking, most of the experiments undertaken by researchers are conducted on manufactured specimens.

The present study investigated seven specimens labeled Shallow Conical Caps (SCC) and seven labeled Deep Conical Caps (DCC) under uniform hydrostatic pressure. Each group contained one perfect specimen, with the remaining specimens having imperfections with amplitudes of 1t, 2t, or 3t (t is the thickness of the conical shell). The failure modes of Maali *et al.*'s 2012 experimental tests are shown in Figure 2.4.

Figure 2.4. Collapse modes in research by Maali *et al.* (2012)

Fatemi *et al.* (2013) investigated imperfect cylindrical shells under uniform external pressure. In this research, the load-carrying behavior of cylindrical thin-walled shell structures under load pressure was strongly dependent on the nature and magnitude of the imperfections invariably caused by various manufacturing/welding processes. Weld-induced geometric imperfections were reported to have especially detrimental effects on the buckling resistance of shells under uniform external pressure.

The buckling and post-buckling capacity of shells depend considerably on the cross-sectional form and depth of the geometric imperfections, and on the H/R and R/t ratios

(H = height, R = radius, and t = thickness of the cylindrical shell). In the present study, we manufactured and tested a series of specimens having 4t and 8t magnitudes of imperfections with different ratios of H/R and R/t. The results of testing under different codes are compared. This study shows a considerable reduction in the buckling resistance of the shells. The collapse mode of Fatemi *et al.*'s (2013) experimental tests are shown in Figure 2.5.

Figure 2.5. Collapse modes of research by Fatemi *et al.* (2013)

Nilufari *et al.* (2014) discussed 12 laboratory specimens in three groups, labeled SP200 [S¼ specimen, P¼ perfect, 200¼ height (mm), and radius of cylinder], SP250 [S¼ specimen, P¼ perfect, 250¼ height (mm), and radius of cylinder] and SP300 [S¼ specimen, P¼ perfect, 300¼ height (mm), and radius of cylinder] loaded under uniform hydrostatic pressure. The samples were modified to include circumferential imperfections at the junctions between the curved edges of the panels of the cylindrical and conical shells, with amplitudes of 2t, 4t, and 8t in depth (where t is the thickness of the conical or cylindrical shell).

The results of testing under different codes are compared. This study shows that geometrical imperfections at different ratios of t/R (where R is the radius of the tanks) may have decreasing, neutral, or increasing effects on the buckling resistance and can result in softening or stiffening behaviors of the shells. The effects of circumferential imperfections caused by continuous welding on the joined areas between the curved panel

edges of the cylindrical and conical shells of steel storage tanks with fixed conical roofs is the most important case in this context. The test model of Nilufari *et al.* (2014) is shown in Figure 2.6.

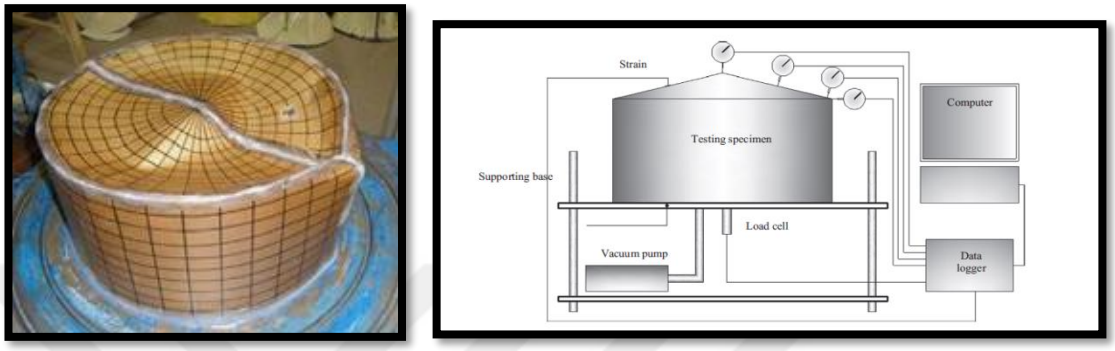

Figure 2.6. Machine test and collapse test in research by Niloufari *et al.* (2014)

Tohid Ghanbari Ghazijahani *et al.* (2014a) studied damaged cylindrical shells under compression. The purpose of this study presented an experimental program in which the buckling and failure response of damaged shell specimens were analyzed. The results of this study can be generalized for many kinds of cylindrical shells to full-scale applications with similar D/t ratios.

Figure 2.7. Experimental test in research by Tohid Ghanbari Ghazijahani *et al.* (2014a)

Tohid Ghanbari Ghazijahani *et al.* (2014b) conducted experiments on dented cylindrical shells under peripheral pressure. They reported on an experimental program on the

buckling and post-buckling response of thin cylindrical shells with local dent imperfections under uniform external pressure. The results of this study can be used in practical structures with similar geometrical features.

Figure 2.8. Experimental test in research by Tohid Ghanbari Ghazijahani *et al.* (2014b)

Tohid Ghanbari Ghazijahani *et al.* (2014c) also conducted a great deal of research in regard to thin shells under external pressure. In some cases, modeled structures were directly subjected to external pressure imposed from outside the surface of these structures, whereas in some cases a vacuum was applied such that the atmospheric pressure played the role of peripheral pressure. Since 1996, Showkati and his research colleagues have conducted many studies in which a uniform external pressure was imposed through an internal vacuum.

Some of these investigations are outlined herein: the effect of boundary conditions on shell structures was studied in. Tohid Ghanbari Ghazijahani *et al.* (2014c) In this study, the authors used the same method of connection with epoxy in the present thin shells, which eventually resulted in a highly satisfactory connection both for longitudinal stiffeners (known as stringers) and thickeners. On the other hand, to the best of the authors' knowledge, no other researchers have employed an end plate attached to one end of the specimen to impose axial stresses to the body of such structures subjected to a vacuum. It is of interest that this geometry leads to a different collapse modes in these structures, and this has not yet been reported. Note that stiffened shells with an end plate are quite widespread in many applications. The end plate takes the role of a cap in such cylindrical shell structures.

Figure 2.9. Experimental test and machine test in research by Tohid Ghanbari Ghazijahani *et al.* (2014c)

Tohid Ghanbari Ghazijahani *et al.* (2015a) focused on recovering the fatigue life for larger cutouts by reinforcement with CFRP. The fatigue life was not only fully recovered with the CFRP reinforcement but also dramatically increased relative to the unreinforced intact specimen. The test model of Tohid Ghanbari Ghazijahani *et al.* (2015) is shown in Figure 2.10.

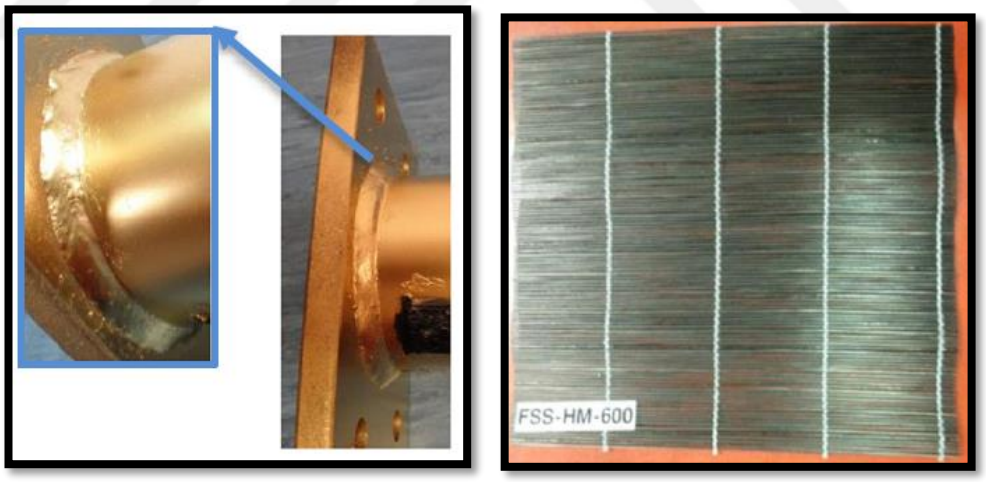

Figure 2.10. Experimental test in research by Tohid Ghanbari Ghazijahani *et al.* (2015a)

In addition, Tohid Ghanbari Ghazijahani *et al.* (2015b) studied a new approach for strengthening in which vertical corrugations were introduced on 11 cylindrical shell specimens under uniform external pressure. The results showed a considerable increase in the buckling capacity of such structures.

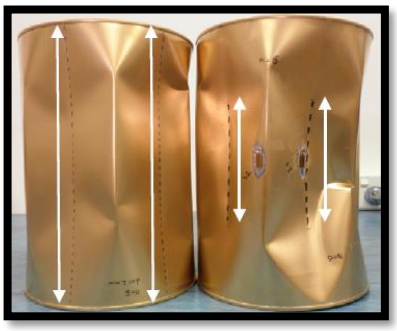

Figure 2.11. Experimental test in research by Tohid Ghanbari Ghazijahani *et al.* (2015b)

Tohid Ghanbari Ghazijahani *et al.* (2015c) studied the effect of large local imperfections, known as dents, on the plastic buckling capacity of short steel tubes under axial compression. A total of 11 tests on such short columns were carried out. The specimens were indented through a separate process, and the ultimate axial capacity was subsequently obtained through compression tests. Dent imperfections with various depths were introduced to different locations on the bodies of the specimens. The plastic buckling modes, as well as the ultimate capacity of the specimens, were thoroughly investigated. The adverse effects of such a local damage on the load-carrying capacity was quantified for different values and types of imperfections.

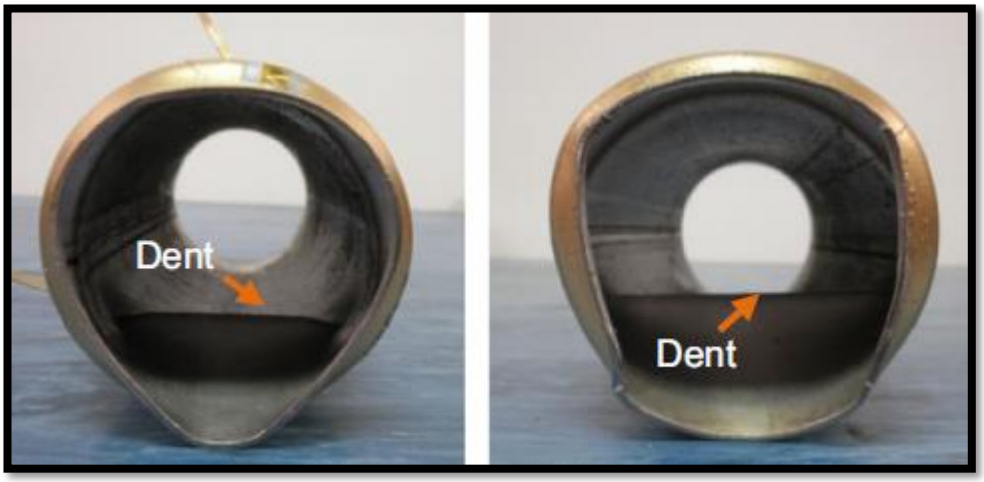

Figure 2.12. Experimental test in research by Tohid Ghanbari Ghazijahani *et al.* (2015c)

Tohid Ghanbari Ghazijahani *et al.* (2015d) discussed the structural behavior of an innovative composite column through an experimental study. The new composite was composed of steel cylindrical hollow sections (CHSs), solid timber infill, and CFRP confinements. The present stub columns were under pure axial compression. The plastic buckling, failure modes, and deformational response of the mentioned elements were assessed. The ultimate capacity enhancement was evaluated for specimens with different conditions, and comprehensive discussions were conducted in order to clarify the effect of each material on the structural behavior of different specimens.

Figure 2.13. Failure mode in research by Tohid Ghanbari Ghazijahani *et al.* (2015d)

Morteza Vakili and Hossein Showkati (2015) studied the inelastic buckling behavior of cylindrical shells near the base, known as elephant-foot buckling. This form of buckling occurs under high internal pressure exerted simultaneously with axial compression. The buckling of cylindrical shells subjected to combined axial loads and internal pressure was

experimentally studied and tested, and a new method of strengthening steel cylindrical shells using FRP composite materials was presented. The proposed method was studied with numerical methods using a nonlinear algorithm, and the results were evaluated for the resistance to buckling of cylindrical shells. The results provided effective and useful information for the retrofitting of cylindrical shell tanks.

Above-mentioned literature review may be concluded as follows. The cylindrical shell is a main structural element and is considered to be a basic need in modern industry. The structures of shells are prone to buckling phenomena owing to their particular shape. The insignificant thickness of the other dimensions, and the emergence of compressive stresses owing to loading, are factors that cause the buckling phenomenon.

In the context of the stability of a cylindrical shell, many theories have been proposed, each based on specific assumptions. These assumptions simplify the governing relationships to obtain sustainability equations which, of course, limit their scope of application. However, owing to the complex formulation of shell theory, it is not easy to obtain the equilibrium and stability equations for these structures under different loading conditions, and in some cases this is practically impossible. With the development of laboratory and numerical methods, it is possible to eliminate the major uncertainties related to the buckling behavior of cylindrical shells.

3. EXPERIMENTAL STUDY

According to research evoleted about thin-walled cylindrical shells, the following specifications were decided as the main concept of this thesis.

3.1. Thin-Walled Cylindric Specimens

In this section, 10 laboratory specimens in two groups with verified dents and horizontal height directions are examined. The first group of specimens (five specimens) labeled without CFRP and the second group with CFRP were loaded under uniform pressure. Each group contained a perfect model and a perfect model with an entire surface of CFRP, with the remaining specimens having a dent with amplitudes of t_c and $2t_c$ (t_c = thickness of the cylindrical shell). A perfect model and a perfect model with entire surface CFRP were used for control in each group. The details of the specimens are presented in Table 3.1 and Figure 3.1. The CFRP strip was calculated with the formula $3b_d \times (L_d + 2b_d)$, where $3b_d$ is the width of the CFRP strip, and $L_d + 2b_d$ is length of the CFRP strip (L_d = dent length, and b_d = dent width).

Table 3.1. Initial geometry of test models

Group	specimen	Dent length L_d	Dent depth h_d	Dent width b_d	CFRP	Dent number
Without CFRP	C1	$h_c/2$	t_c	$2t_c$	-	2
	C2	$h_c/3$	t_c	$2t_c$	-	2
	C3	$h_c/2$	$2t_c$	$4t_c$	-	2
	C4	$h_c/3$	$2t_c$	$4t_c$	-	2
	C5	Perfect model				
with CFRP	C6	$h_c/2$	t_c	$2t_c$	$3b_d \times (ld + 2b_d)$	2
	C7	$h_c/3$	t_c	$2t_c$	$3b_d \times (ld + 2b_d)$	2
	C8	$h_c/2$	$2t_c$	$4t_c$	$3b_d \times (ld + 2b_d)$	2
	C9	$h_c/3$	$2t_c$	$4t_c$	$3bd \times (ld + 2b_d)$	2
	C10	perfect model with entire-surface CFRP				

Height of cylindrical shell = h = 500 mm, dent length = Ld = h/2 = 250 mm, and h/3 = 166.67 mm. Thickness of cylindrical shell = tc = 1 mm. Radius = R = 500 mm.

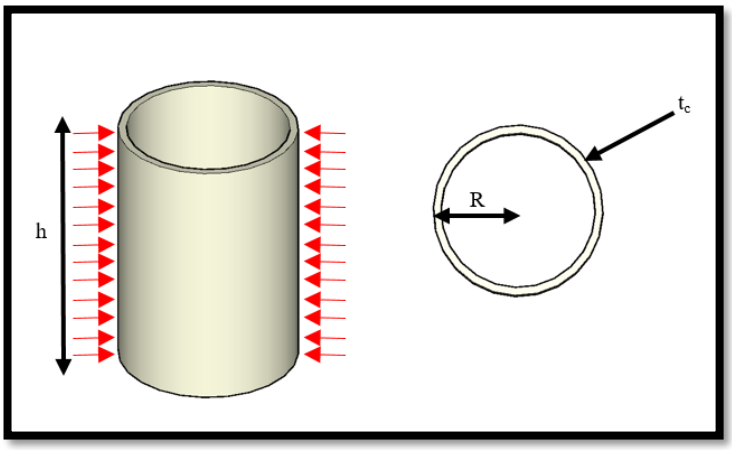

Figure 3.1. Details of experimental test model

3.2. Test Setup and Dent Implementation

The test machine consists of two plates: upper and bottom plates with dimensions of 1500 × 1500 mm and with a plate thickness of 30 mm. The plates were first cut into 1500 × 1500-mm sizes by a CNC cutting device, then ring-cut with a CNC cutting machine. After that, the ring was welded to plates. Fig. 3.2 shows the test machine used for this research. In one of the plates on the upper part, there are two holes in the middle of the passage of the vacuum hose from the first hole. The load cell is inserted into the second hole, and four sets of studs on the four sides of the plate lift the plate with a welding crane.

On the sides of the plates, three holes of the bolt are intended to be six in total, until the configuration shown in Figure 3.2 is achieved. The reason for these six bolts is the installation of a top plate assembly, which, when tested with the crane, prevents these bolts from entering the axial load into the cylinder.

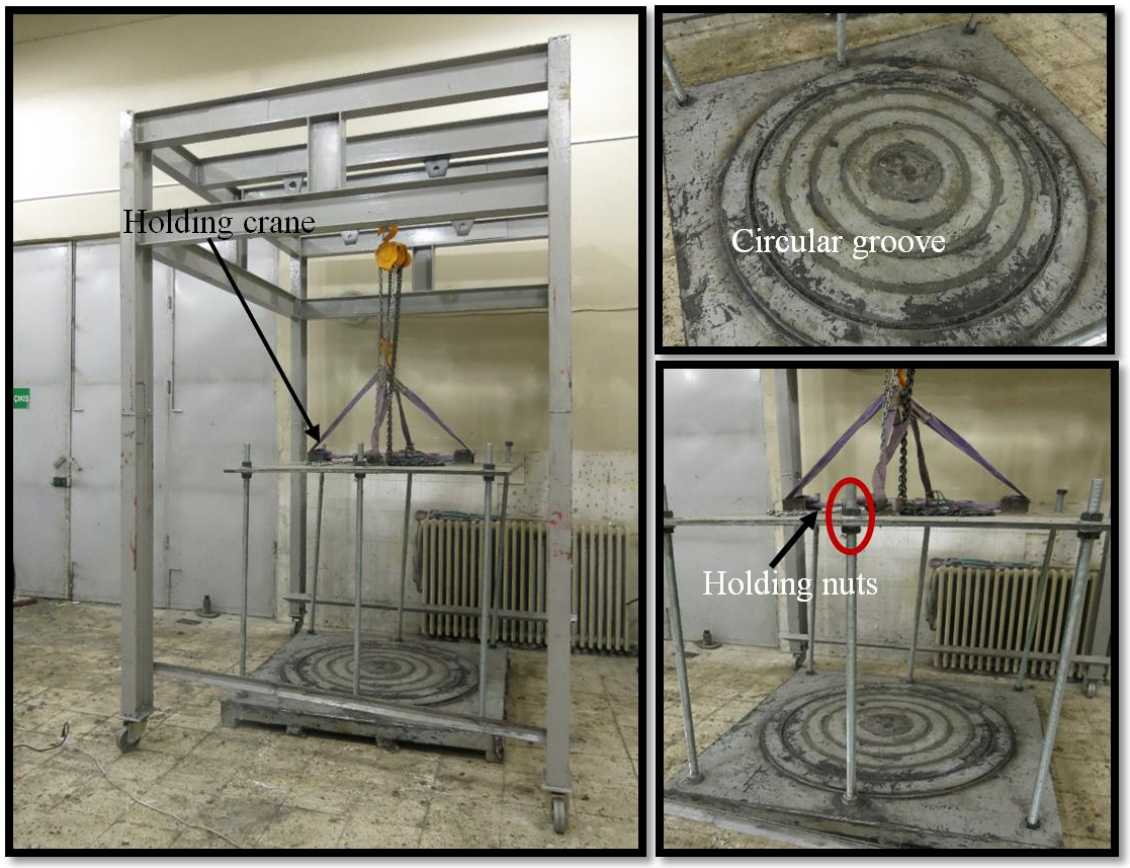

Figure 3.2. Detail of test machine and crane

After the test machine was manufactured, it was time to build laboratory samples. Three tensile coupon tests were performed to obtain the material properties. The average yield and failure stresses were found to be 198.8 MPa and 342.4 MPa, respectively. Young's modulus was calculated as 210 MPa, and Poisson's ratio was obtained as 0.29. To make samples, sheets with a thickness of 1 mm were prepared. Ten sheets were cut to 500 mm in height and 3140 mm in length with scissors. Then, a cylindrical roller was used to create rolled specimens. After that, all specimens were test welded with an argon welding machine.

During the welding, it was considered that the least porosity and inadequacy of welding on the laboratory models were not created, and the models were prepared without imperfections in welding. In addition, during rolling, we were careful not to cause any imperfections.

After the creation of the laboratory models, it was necessary to create inadequacies. In order to create disadvantages in the models, stainless steel shapes (SPKR) were made in the form of cutting and the wire cut method. Until it was executed on dent laboratory models. Figure 3.3 shows the dent piece for the experimental tests.

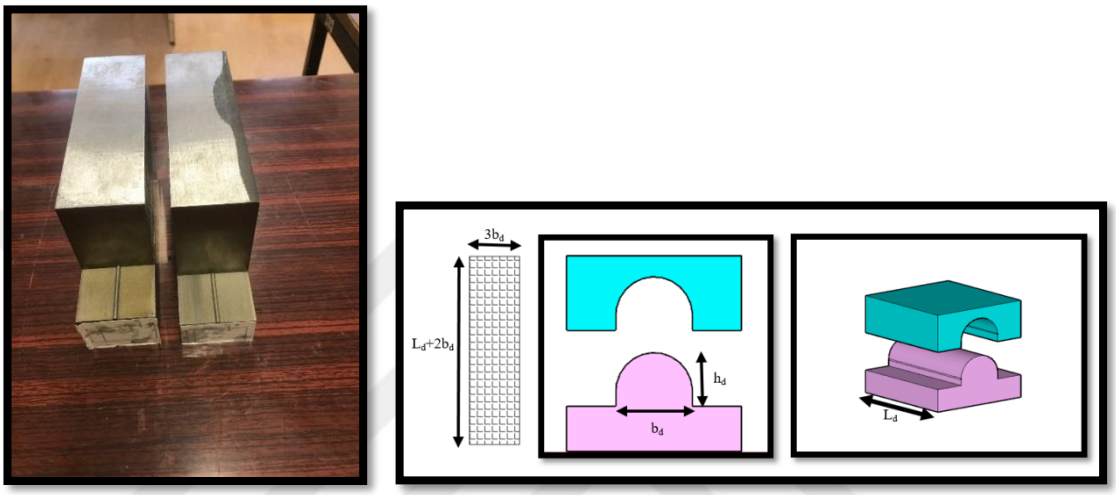

Figure 3.3. Dent piece and CFRP detail

First, a dent length was indicated on the model with a ruler and a marker, and then a four-base was laid inside the model. A static load pump was employed with a maximum 900-kN load, a maximum stroke of 300 mm, and a constant speed of 0.016 mm/s. The pump was used to obtain dents in the models (Maali *et al.* 2016 and 2017). In Figure 3.4 the dent implementation was observed in the models.

Figure 3.4. Dent implementation of the models

For the group with CFRP models that were to be used (CFRP), two-component epoxy-coated (CFRP) adhesive was stuck onto the specified parts. Table 3.1 lists data for the experimental models.

To install the laboratory models, the following was accomplished:

1- Beginning at the bottom of the laboratory model, after fitting the model on the bottom plate of the silicone silencer model, it was filled to the plate inside and outside the cylinder to prevent air from escaping from the inside of the cylinder.

2- To fit the other side of the cylinder, the bolts around the device were opened, and the slowly raised upper plate was guided by a crane to the cylinder. Prior to guiding the top plate, the bolts were adjusted to the height of the cylinder to prevent a sudden collision of the plate with the cylindrical model.

3- After inserting the top plate, the bolt shown in Fig. 3.2 was closed to prevent gravity loading on the cylindrical model. After the placement of the plate around the cylinder was filled with silicon glue, silicon was added to prevent air escape.

After performing the above steps, four metal support rings, two on the bottom and two on the top of the cylinder as shown in Figure 3.5, were installed so that all laboratory models with a simple support were closed only in the radial direction.

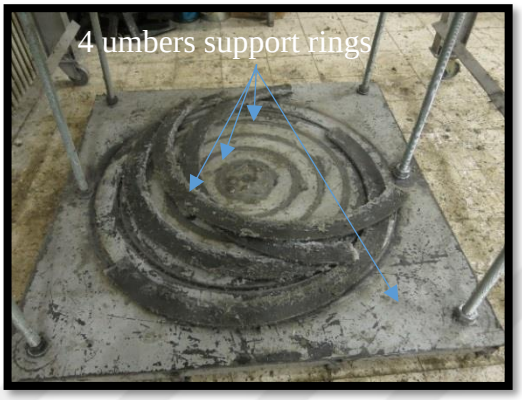

Figure 3.5. Support rings of test machine

To carry out a vacuum pump test, a vacuum pump manufactured by Zinisan had a hydrostatic pressure capacity of 600 kPa. Fig. 3.6 shows the vacuum pump used in the experimental tests.

Figure 3.6. Vacuum pump of experimental tests

4 LVDTs were installed to measure vertical displacements at 0, 90, 180 and 270º at elevations (H/2). Labels of the LVDT were LV1, LV2, LV3, and LV4. These four LVDTs

were 300 mm in length and were of the Japanese SDP-300 type. The error of the LVDT was 0.001 mm. During the test, we connected all four LVDTs to prevent magnetization overturned to the base. Figure 3.7 shows the LVDTs.

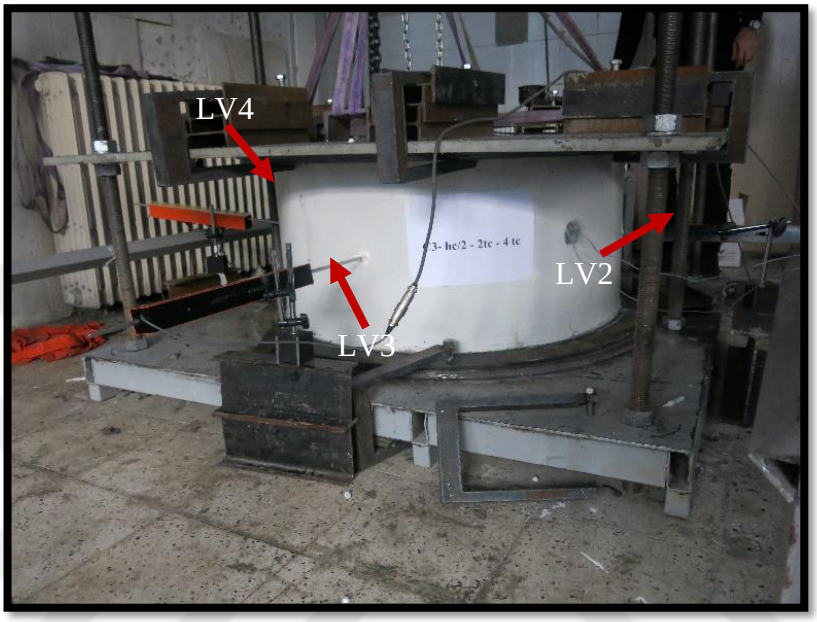

Figure 3.7. Linear Variable Displacement Transducers (LVDTs)

In all experiments, two strain gauges (S1 = vertically and S2 = horizontally) were installed. Table 3.2 lists the locations of the strain gauges. Before installing the strain gauge, we placed them thoroughly with a flap and then, after cleaning, with a special adhesive on the desired area. The strain gauges were of the type YEFLA-5. Their resistance was 121Ω ± 0.5%, the coefficient of sensitivity was 2.1 ± 2%, and their size was 5 mm × 3 mm. This is shown in figure 3.8.

Table 3.2. Layout of strain gauges for all test specimens.

Group	Specimen label	Strain gages	
		S1º Height (mm)	S2º Height (mm)
without CFRP	C1	93	94
		220	220
	C2	100	101
		210	210
	C3	118	119
		250	250
	C4	100	101
		180	180
	C5	120	121
		220	220
with CFRP	C6	120	121
		250	250
	C7	116	117
		245	245
	C8	130	131
		250	250
	C9	115	116
		250	250
	C10	110	111
		230	230

Figure 3.8. S1 and S2 strain gauges

To collect the experimental results, a data logger was used: the INSTURUNET 1420 model with 120 channels and 13 inputs. The logger transmitted information to a computer, as shown in Figure 3.9.

Figure 3.9. Data logger

4. RESULTS AND DISCUSSIONS

Except the two models with and without CFRP, eight cylindrical thin walled short cylinders are tested throughout this study. The results of ten samples are presented within this chapter. The bad-displacement, load-strain, initial buckling, overall buckling, buckling collages, waves were observed experimentally and theoretically.

4.1. Without CFRP Group

4.1.1. Test sample C1

As noted above, this specimen is made of sheet with a thickness of 1 mm, a height of 500 mm, and a radius of 500 mm. This sample has a dent to a depth of t_c and a width of $2t_c$ with a height of the dent of h/2. During the test, the pressure drop does not exceed 0.1 kPa. At around 67.54 kPa, a very loud sound was emitted. Then, waves were formed one after the other, and finally, 10 waves were generated in the sample. The buckling load reached 123.06 kPa. After the final buckling, the ٧-٨ and ٧-٨ failures moved up and down, eventually reaching 188.32 KPa with a collapse buckling load. The experiment ended during the lifting of the cylinder's edge and an air leak. Figs. 4.1 and 4.2 show the load-displacement and load-strain curves for the models, and Figs. 4.3 and 4.4 show the models before and after the tests.

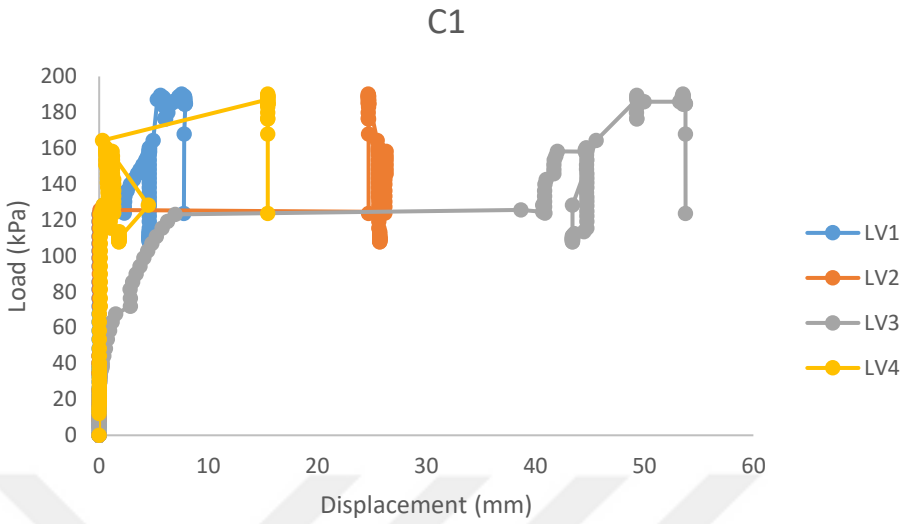

Figure 4.1. Load-Displacement for the C1 model

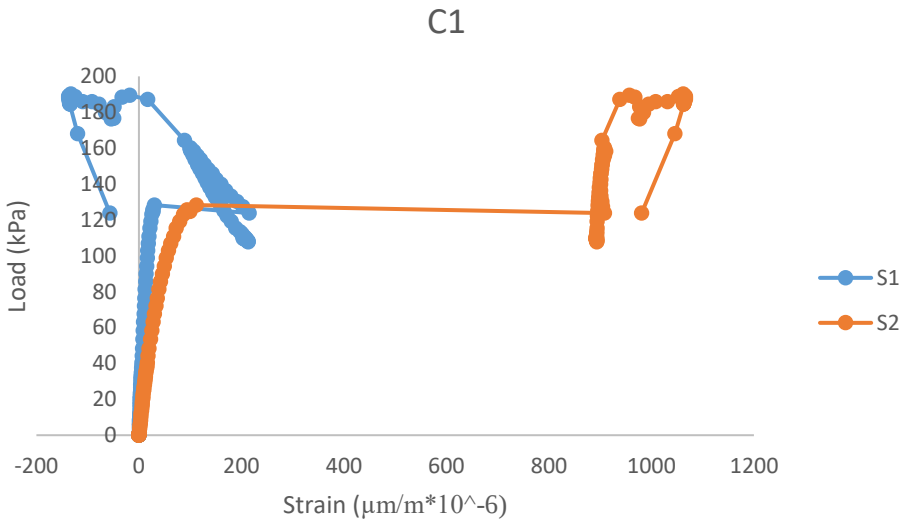

Figure 4.2. Load-Strain for the C1 model

Figure 4.3. The C1 model before test

Figure 4.4. The C1 model after test

4.1.2. Test sample C2

As noted above, this specimen is made of sheet with a thickness of 1 mm, a height of 500 mm, and a radius of 500 mm. This sample has a dent to a depth of t_c and a width of $2t_c$ with a height of the dent of h/3. During the test, the pressure drop does not exceed 0.1 kPa. At around 88.25 kPa, a very loud sound was emitted. Then, waves were formed one after the other, and finally, 8 waves were generated in the sample. The buckling load reached 119.67 kPa. After the final buckling, the ٧-٨ and ٧-٨ failures moved up and down, eventually reaching 214.05 KPa with a collapse buckling load. The experiment ended during the lifting of the cylinder's edge and an air leak. Figs. 4.5 and 4.6 show the load-displacement and load-strain curves for the models, and Figs. 4.7 and 4.8 show the models before and after the tests.

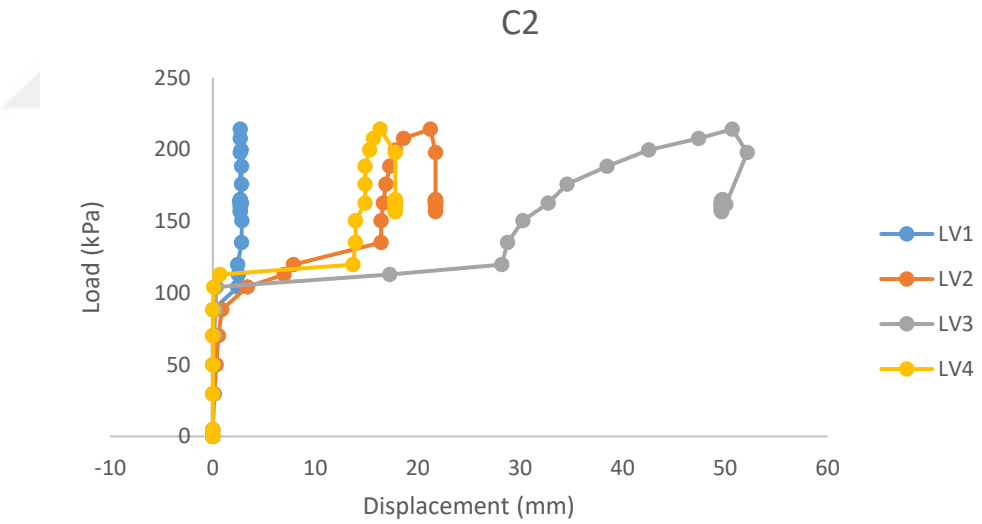

Figure 4.5. Load-Displacement for the C2 model

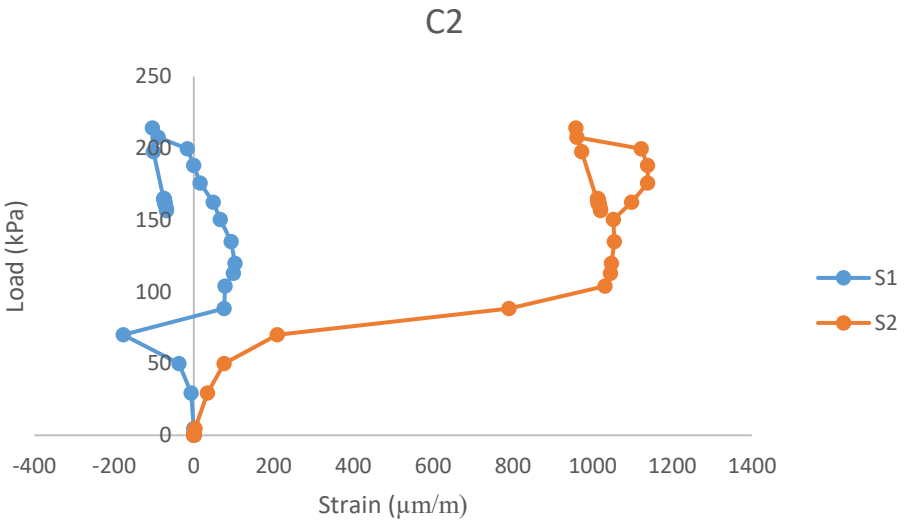

Figure 4.6. Load-Strain for the C2 model

Figure 4.7. The C2 model before test

Figure 4.8. The C2 model after test

4.1.3. Test sample C3

As noted above, this specimen is made of sheet with a thickness of 1 mm, a height of 500 mm, and a radius of 500 mm. This sample has a dent to a depth of $2t_c$ and a width of $4t_c$ with a height of the dent of h/2. During the test, the pressure drop does not exceed 0.1 kPa. At around 82.36 kPa, a very loud sound was emitted. Then, waves were formed one after the other, and finally, 8 waves were generated in the sample. The buckling load reached 135.01 kPa. After the final buckling, the ٧-٨ and ٧-٨ failures moved up and down, eventually reaching 231.08 KPa with a collapse buckling load. The experiment ended during the lifting of the cylinder's edge and an air leak. Figs. 4.9 and 4.10 show the load-displacement and load-strain curves for the models, and Figs. 4.11 and 4.12 show the models before and after the tests.

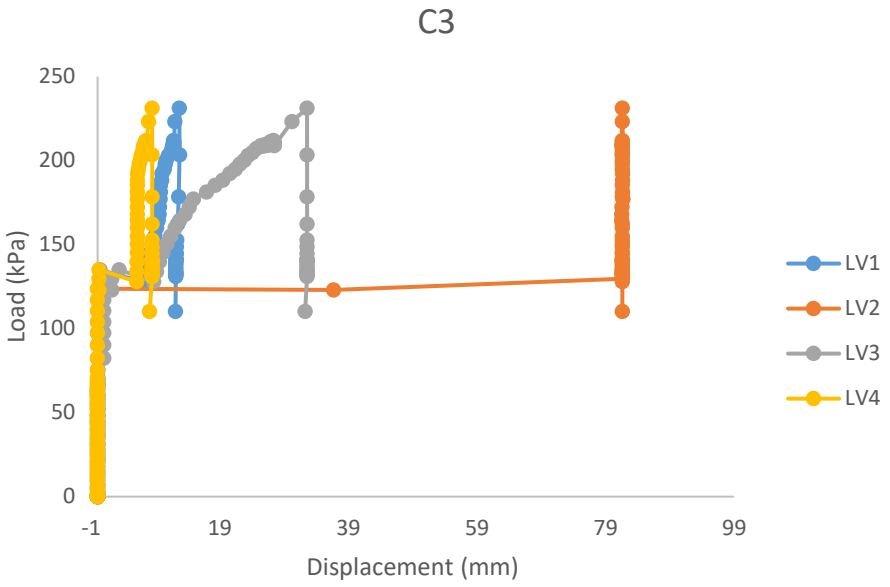

Figure 4.9. Load-Displacement for the C3 model

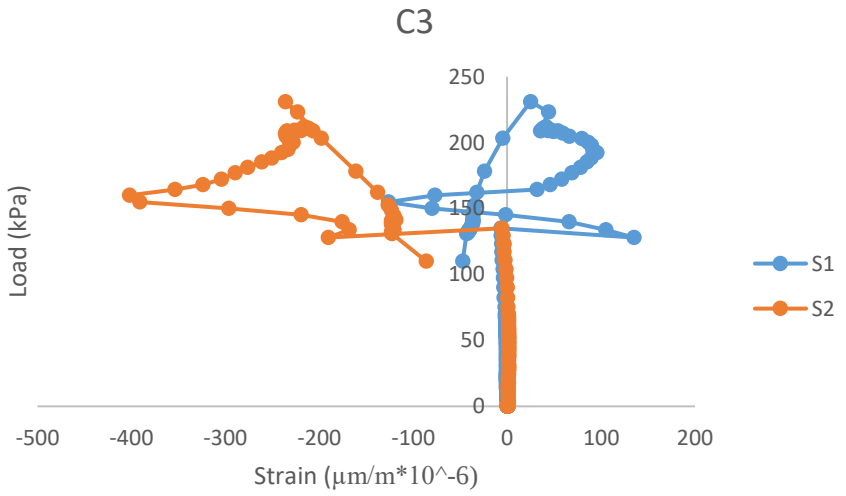

Figure 4.10. Load-Strain for the C3 model

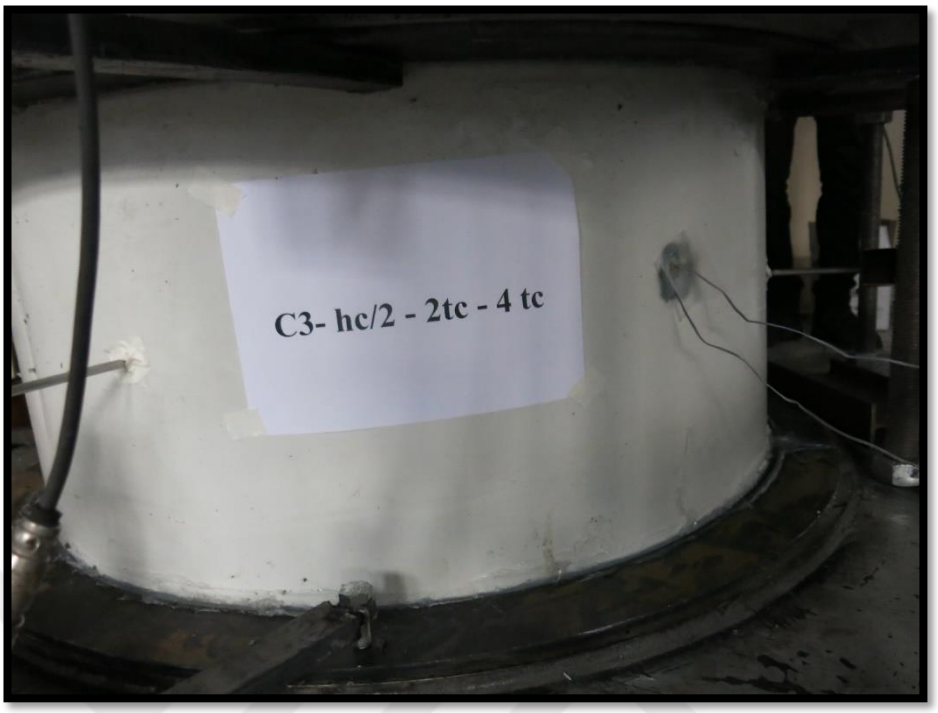

Figure 4.11. The C3 model before test

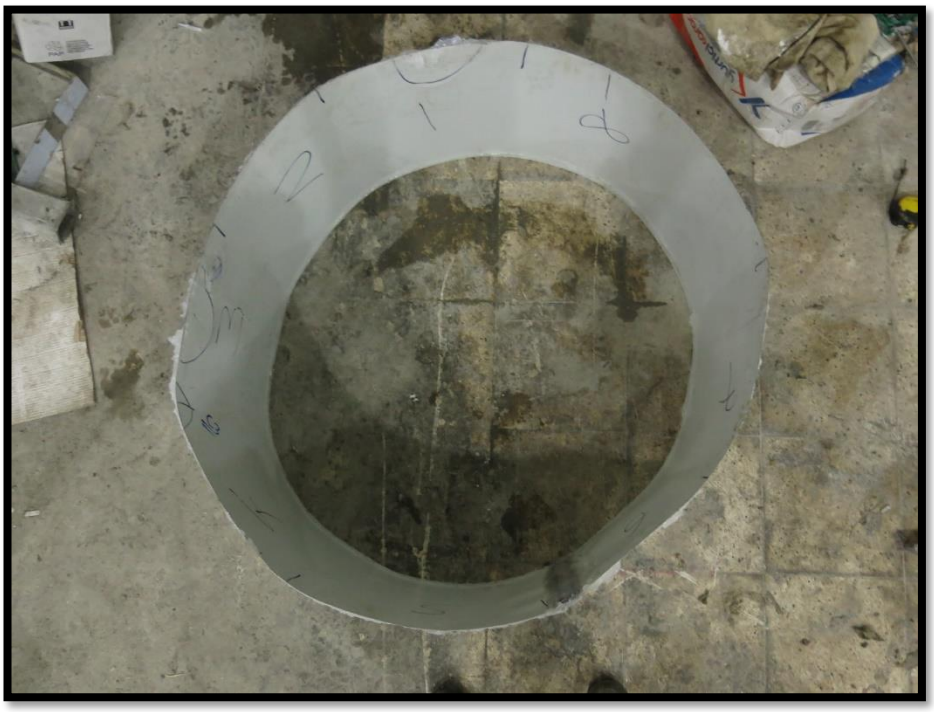

Figure 4.12. The C3 model after test

4.1.4. Test sample C4

As noted above, this specimen is made of sheet with a thickness of 1 mm, a height of 500 mm, and a radius of 500 mm. This sample has a dent to a depth of $2t_c$ and a width of $4t_c$ with a height of the dent of h/3. During the test, the pressure drop does not exceed 0.1 kPa. At around 88.92 kPa, a very loud sound was emitted. Then, waves were formed one after the other, and finally, 8 waves were generated in the sample. The buckling load reached 139.28 kPa. After the final buckling, the ٧-٨ and ٧-٨ failures moved up and down, eventually reaching 275.61 KPa with a collapse buckling load. The experiment ended during the lifting of the cylinder's edge and an air leak. Figs. 4.13 and 4.14 show the load-displacement and load-strain curves for the models, and Figs. 4.15 and 4.16 show the models before and after the tests.

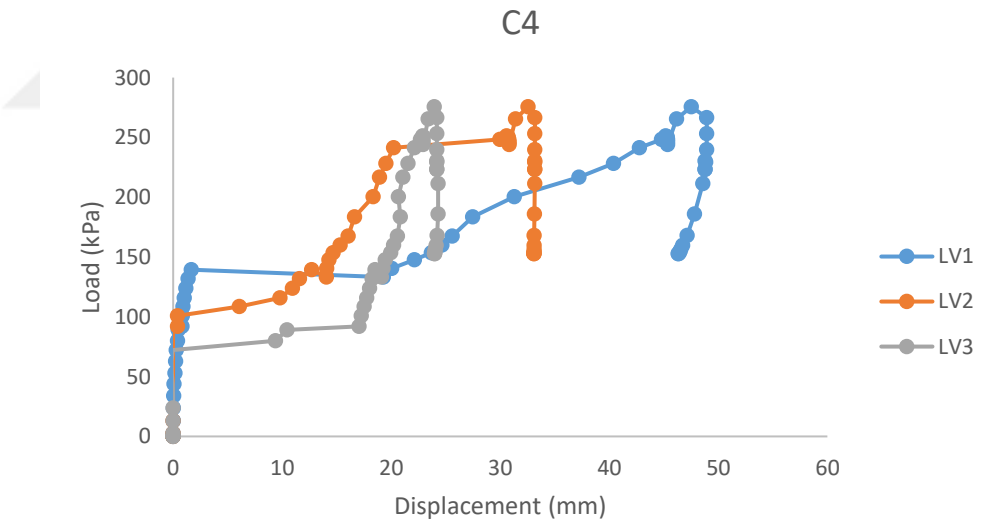

Figure 4.13. Load-Displacement for the C4 model

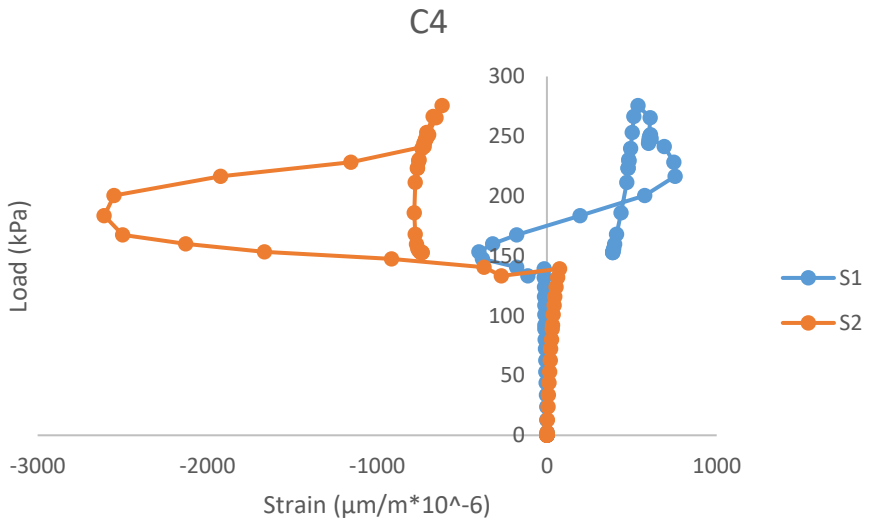

Figure 4.14. Load-Strain for the C4 model

Figure 4.15. The C4 model before test

Figure 4.16. The C4 model after test

4.1.5. Test sample C5 (perfect model)

As noted above, this specimen is made of sheet with a thickness of 1 mm, a height of 500 mm, and a radius of 500 mm. This sample has no dent (perfect model). During the test, the pressure drop does not exceed 0.1 kPa. At around 121.66 kPa, a very loud sound was emitted. Then, waves were formed one after the other, and finally, 9 waves were generated in the sample. The buckling load reached 177.40 kPa. After the final buckling, the ٧-٨ and ٧-٨ failures moved up and down, eventually reaching 269.64 KPa with a collapse buckling load. The experiment ended during the lifting of the cylinder's edge and an air leak. Figs. 4.17 and 4.18 show the load-displacement and load-strain curves for the models, and Figs. 4.19 and 4.20 show the models before and after the tests.

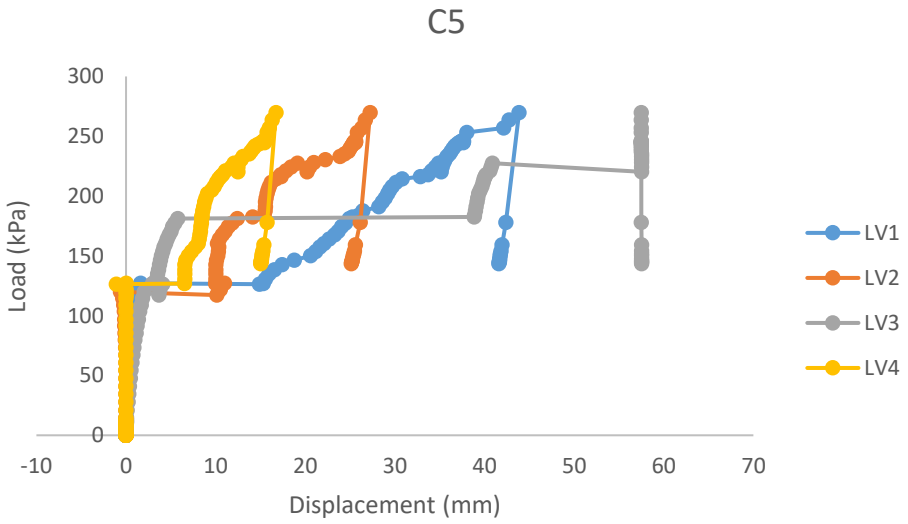

Figure 4.17. Load-Displacement for the C5 model

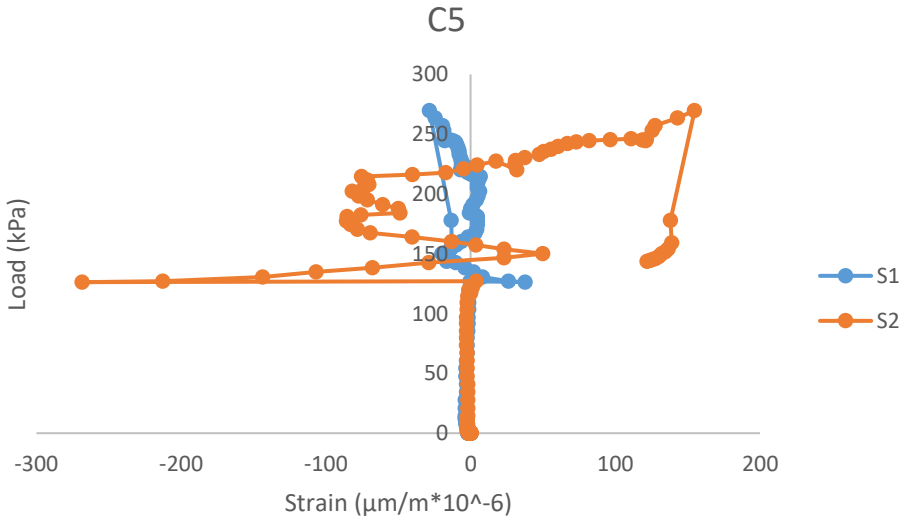

Figure 4.18. Load-Strain for the C5 model

Figure 4.19. The C5 model before test

Figure 4.20. The C5 model after test

4.2. With CFRP Group

The dented and no-dented five samples with CFRP are presented within this section.

4.2.1. Test sample C6

As noted above, this specimen is made of sheet with a thickness of 1 mm, a height of 500 mm, and a radius of 500 mm. This sample has a dent to a depth of t_c and a width of $2t_c$, with a height of dent h/2. The CFRP used in the dent location has dimensions of $3b_d \times (L_d + 2\ b_d)$. During the test, the pressure drop does not exceed 0.1 kPa. At around 90.47 kPa, a loud sound was emitted. Then, waves were formed one after the other, and finally, 8 waves were generated in the sample. The buckling load reached 125.57 kPa. After the final buckling, the ٧-٨ and ٧-٨ failures moved up and down, eventually reaching 195.62 KPa with a collapse buckling load. The experiment ended owing to the lifting of the cylinder's edge and an air leak. Figs. 4.21 and 4.22 show the load-displacement and load-strain curves of the models, and Figs. 4.23 and 4.24 show the models before and after the tests.

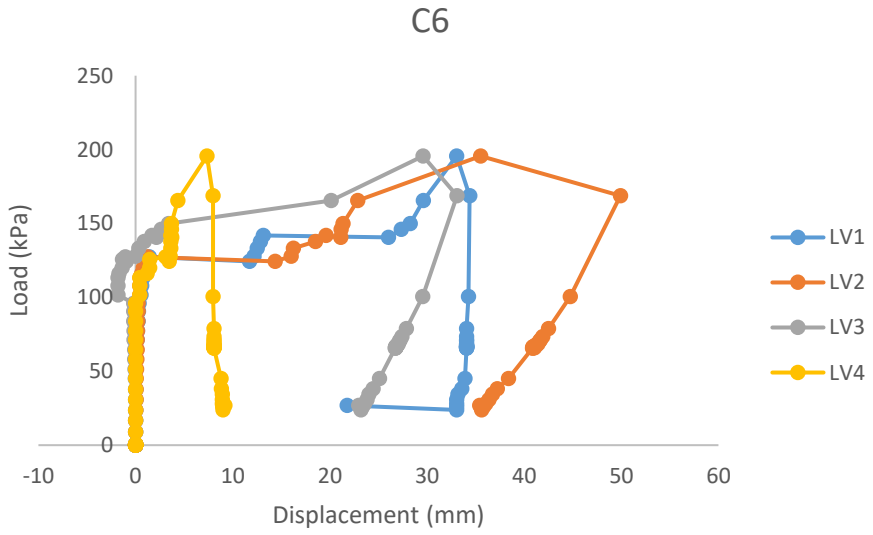

Figure 4.21. Load-Displacement for the C6 model

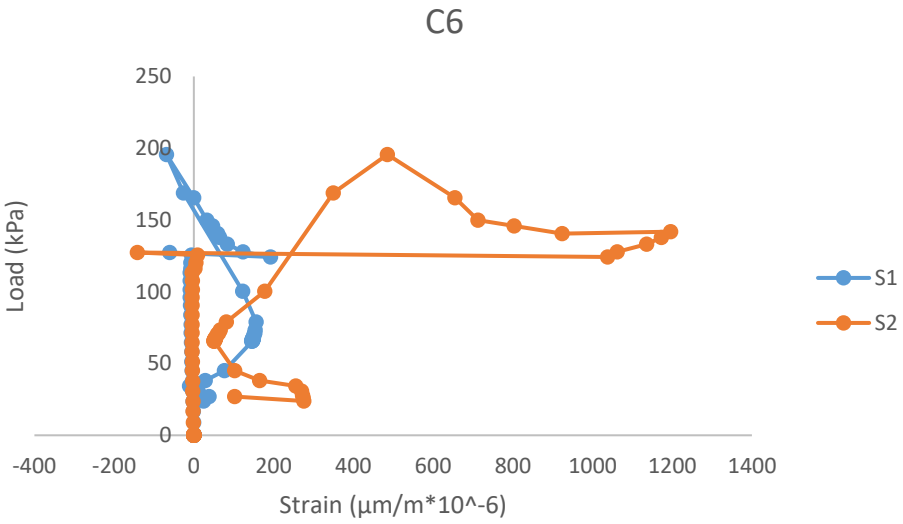

Figure 4.21. Load-Strain for the C6 model

Figure 4.22. The C6 model before test

Figure 4.23. The C6 model after test

4.2.2. Test sample C7

As noted above, this specimen is made of sheet with a thickness of 1 mm, a height of 500 mm, and a radius of 500 mm. This sample has a dent to a depth of tc and a width of $2t_c$, with a height of dent h/3. The CFRP used in the dent location has dimensions of $3b_d \times (L_d + 2\ b_d)$. During the test, the pressure drop does not exceed 0.1 kPa. At around 98.58 kPa, a loud sound was emitted. Then, waves were formed one after the other, and finally, 8 waves were generated in the sample. The buckling load reached 122.54 kPa. After the final buckling, the ۷-۸ and ۷-۸ failures moved up and down, eventually reaching 194.21 KPa with a collapse buckling load. The experiment ended owing to the lifting of the cylinder's edge and an air leak. Figs. 4.24 and 4.25 show the load-displacement and load-strain curves of the models, and Figs. 4.26 and 4.27 show the models before and after the tests.

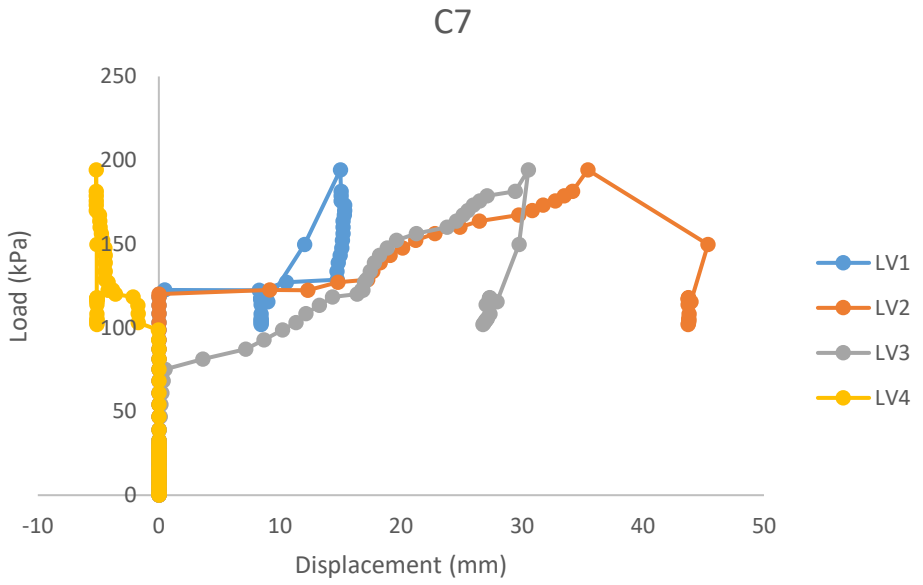

Figure 4.24. Load-Displacement for the C7 model

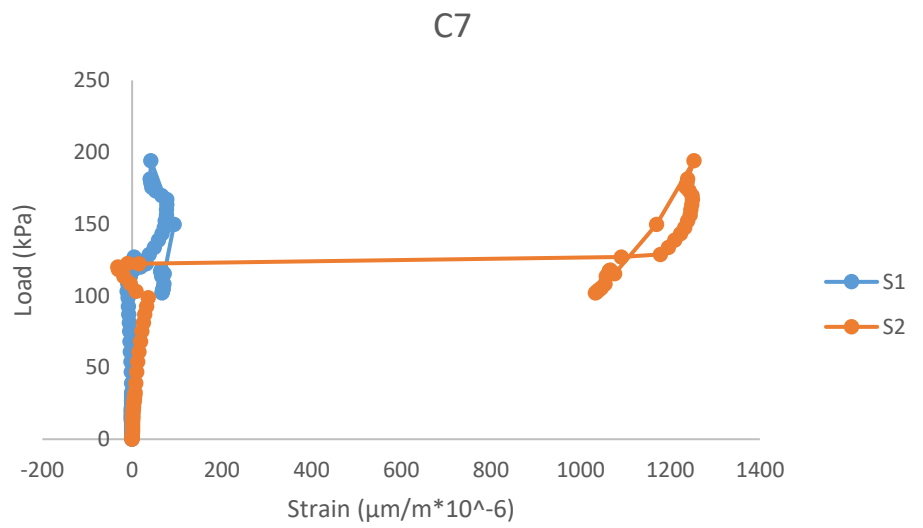

Figure 4.25. Load-Strain for the C7 model

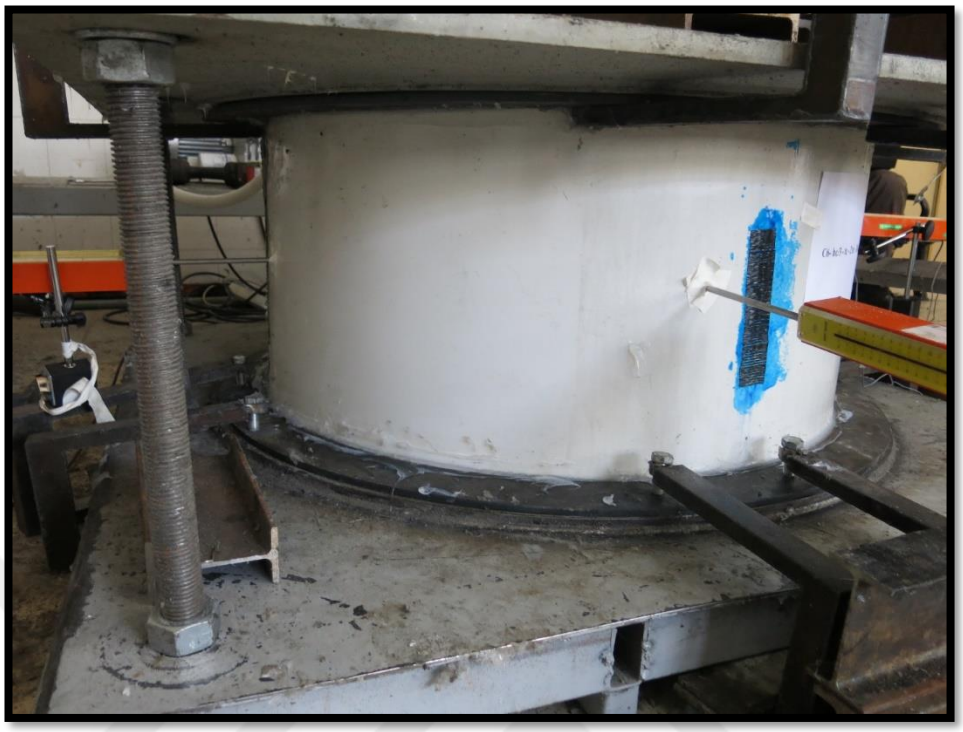

Figure 4.26. The C7 model before test

Figure 4.27. The C7 model after test

4.2.3. Test sample C8

As noted above, this specimen is made of sheet with a thickness of 1 mm, a height of 500 mm, and a radius of 500 mm. This sample has a dent to a depth of $2t_c$ and a width of $4t_c$, with a height of dent h/2. The CFRP used in the dent location has dimensions of $3b_d \times (L_d + 2\ b_d)$. During the test, the pressure drop does not exceed 0.1 kPa. At around 108.38 kPa, a loud sound was emitted. Then, waves were formed one after the other, and finally, 9 waves were generated in the sample. The buckling load reached 181.31 kPa. After the final buckling, the ٧-٨ and ٧-٨ failures moved up and down, eventually reaching 208.88 KPa with a collapse buckling load. The experiment ended owing to the lifting of the cylinder's edge and an air leak. Figs. 4.28 and 4.29 show the load-displacement and load-strain curves of the models, and Figs. 4.30 and 4.31 show the models before and after the tests.

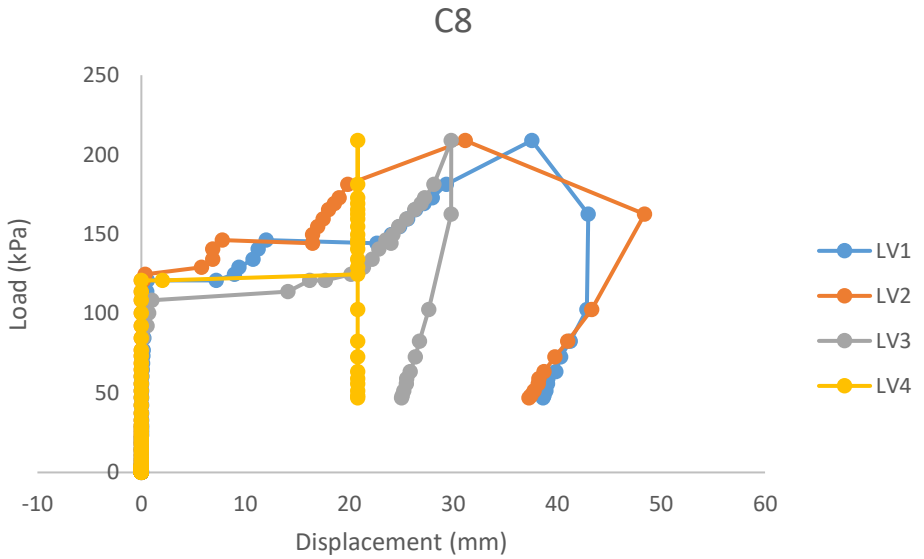

Figure 4.28. Load-Displacement for the C8 model

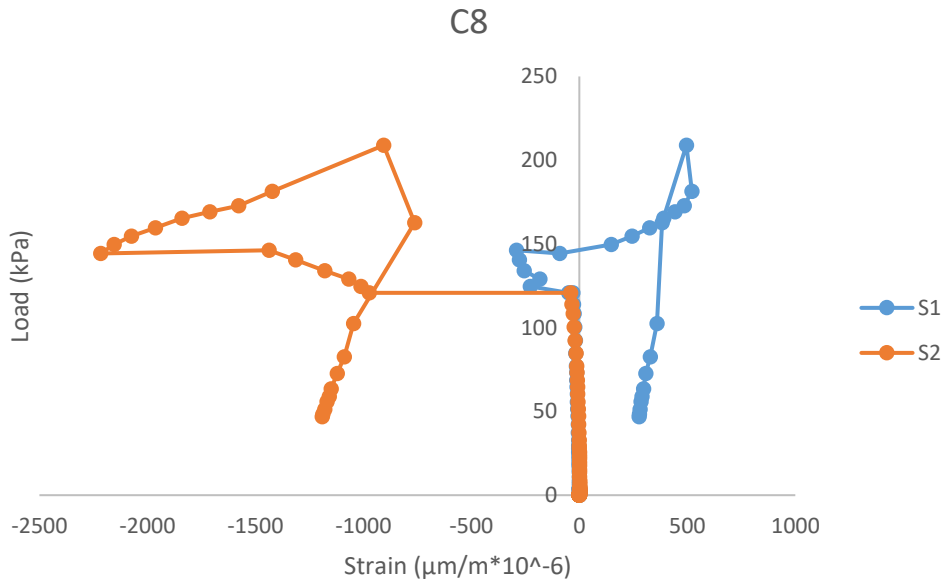

Figure 4.29. Load-Strain for the C8 model

Figure 4.30. The C8 model before test

Figure 4.31. The C8 model after test

4.2.4. Test sample C9

As noted above, this specimen is made of sheet with a thickness of 1 mm, a height of 500 mm, and a radius of 500 mm. This sample has a dent to a depth of $2t_c$ and a width of $4t_c$, with a height of dent h/3. The CFRP used in the dent location has dimensions of $3b_d \times (L_d + 2\ b_d)$. During the test, the pressure drop does not exceed 0.1 kPa. At around 118.26 kPa, a loud sound was emitted. Then, waves were formed one after the other, and finally, 9 waves were generated in the sample. The buckling load reached 174.52 kPa. After the final buckling, the ٧-٨ and ٧-٨ failures moved up and down, eventually reaching 203.14 KPa with a collapse buckling load. The experiment ended owing to the lifting of the cylinder's edge and an air leak. Figs. 4.32 and 4.33 show the load-displacement and load-strain curves of the models, and Figs. 4.34 and 4.35 show the models before and after the tests.

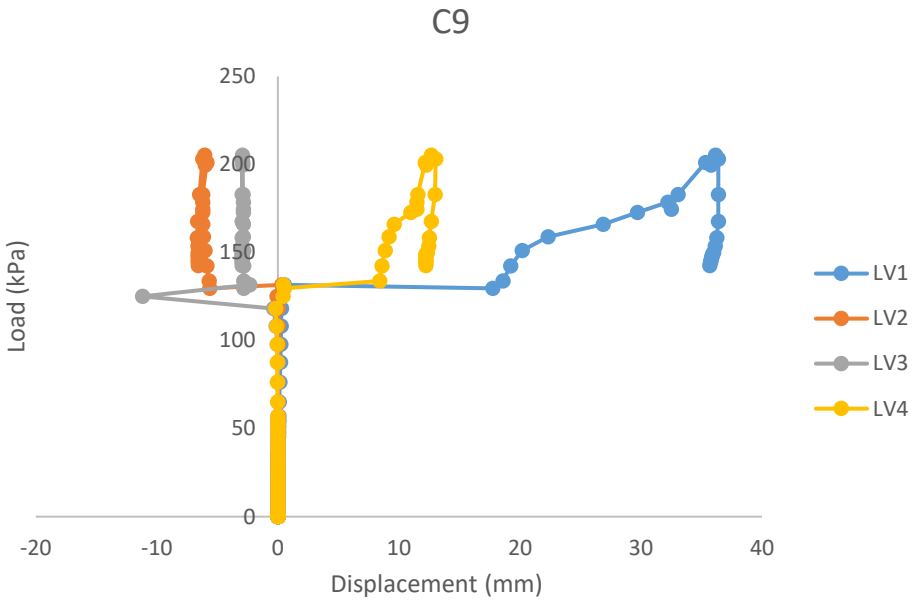

Figure 4.32. Load-Displacement for the C9 model

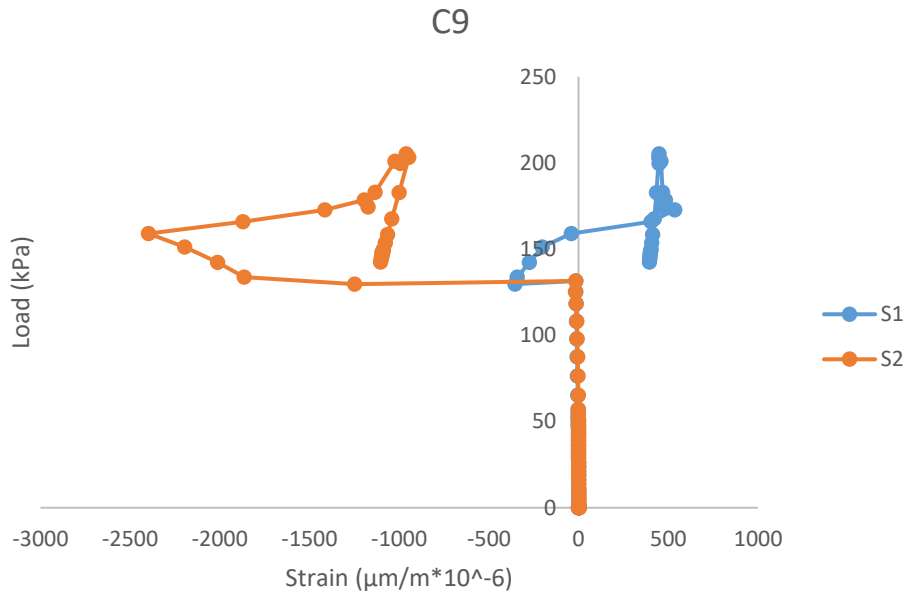

Figure 4.33. Load-Strain for the C9 model

Figure 4.34. The C9 model before test

Figure 4.35. The C9 model after test

4.2.5. Test sample C10 (perfect model with entire-surface CFRP)

As noted above, this specimen is made of sheet with a thickness of 1 mm, a height of 500 mm, and a radius of 500 mm. This sample has with entire-surface CFRP. During the test, the pressure drop does not exceed 0.1 kPa. At around 132.94 kPa, a loud sound was emitted. Then, waves were formed one after the other, and finally, 7 waves were generated in the sample. The buckling load reached 186.32 kPa. After the final buckling, the ٧-٨ and ٧-٨ failures moved up and down, eventually reaching 280.70 kPa with a collapse buckling load. The experiment ended owing to the lifting of the cylinder's edge and an air leak. Figs. 4.36 and 4.37 show the load-displacement and load-strain curves of the models, and Figs. 4.38 and 4.39 show the models before and after the tests.

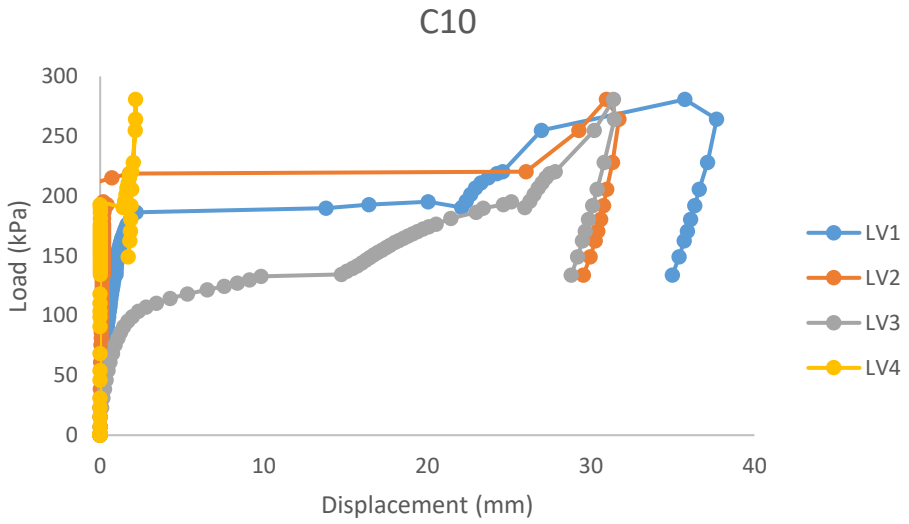

Figure 4.36. Load-Displacement for the C10 model

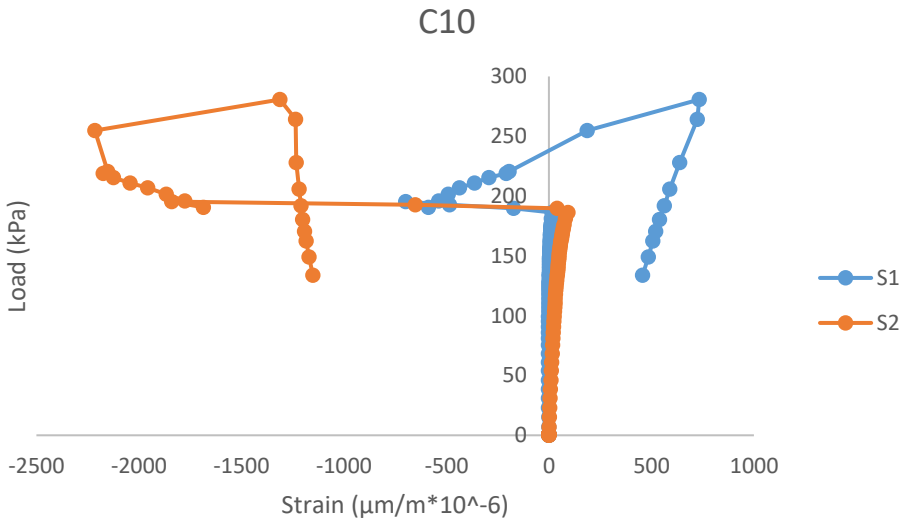

Figure 4.37. Load-Strain for the C9 model

Figure 4.38. The C10 model before test

Figure 4.39. The C10 model after test

4.3. Comparison of First Group (Without CFRP)

In this section, we first compare the models with the same penetration depth (C1 model with C2 model and C3 model with C4 model). In the case of initial loading, with an increasing livestock length from h/3 to h/2, the initial loading was 23.47 and 7.38% for the C2 models and from C1 and C4 to C3, respectively. In addition, for the overall buckling load, it can be said that with an increase in the exit length from h/3 to h/2, the overall buckling in the C2 model was increased to 83.8%, while for the C4 and C3 models, the final value was 3.06%.

With an increase in the length of the dent from h/3 to h/2, the collapse load decreased by 12.02% and 16.16%, respectively, for the C2 models relative to C1 and C4, respectively, of C3. In this group, the buckling load decreases with increasing amplitude at the same depth of penetration.

At present, according to Table 4.1, the models with the same lengths of valves and different dent depths (C1 compared to the C3 model, and the C2 model relative to the C4 model). For the initial load, by increasing the dent depth from tc to $2t_c$, the initial buckling load is increased by 17.99% and 0.75% for the C1 model, respectively, compared to the C3 model and the C2 model, respectively, from model C4. For the overall buckling load, this percent increased by 9.8% and 14.08%, respectively, for the C1 model compared with the C3 and C2 models and C4. This represents an increase of 18.50% and 22.33% for the collapse load.

It can be concluded that models with same dent lengths and dent depths are different with increasing dent depths, and the model is strengthened. And the depth of penetration, the dent is a booster element for the model. On the other hand, if the initial loading load and flexural failure of each model are compared to ours, the overall load buckling compared to the initial buckling load of 2.78, 2.45, 2.81, 3.1, and 2.22 for the C1, C2, C3, C4, and C5 models, respectively. After the initial load buckling of the models, they resisted the models themselves. They entered the stage of post buckling. A fading effect is seen in all models.

In general, the collapse load is about 2.5 times the initial load buckling. Now, if we compare the perfect sample C5 with the other test models according to Table 4.1, for C5's initial buckling load and the C1–C4 models, we can say this increased by 44.48, 27.46, 32.54, and 26.91%, respectively. The overall buckling increased by 30.63, 32.54, 23.89, and 21.48%, respectively. For collapse buckling, the load increased by 30.15, 20.61, and 14.30%, respectively, compared to the C1, C2 and C3 models. The collapse buckling load decreased by 2.21% over the C4 model.

4.4. Comparison of Second Group (With CFRP)

In this section, we first compare the models with the same penetration depth (C6 model with C7 model and C8 model with C9 model). In the case of initial loading, with an increasing dent length from h/3 to h/2, the initial loading was 8.23 and 8.35% for the C7

models, respectively, from C6 and C9 to C8, respectively. In addition, for the overall buckling load, with an increase in exit length from h/3 to h/2, the overall buckling for the C7 model was decreased to 2.47%, while for the C6, for the C9 model was decreased to 3.89%, while for the C8 model.

With regard to the collapse load, with an increase in the length of the dent from h/3 to h/2, the collapse load decreased by 0.07% and 2.79%, respectively, for the C7 models relative to C6 and C9, respectively, of C8. For example, in this group, the buckling load decreased with increasing amplitude at the same depth of penetration. At present, according to Table 4.1, models with the same lengths of valves and different dent depths (C6 compared to the C8 model and the C7 model relative to the C9 model).

In the case of initial load, by increasing the dent depth from tc to 2tc, the initial buckling load increased by 16.53% and 16.64% for the C6 model, respectively, compared to the C8 model and the C7 model, respectively, from model C9. For the overall buckling load, this percentage increased by 30.74% and 29.78%, respectively, for the C6 model compared with the C8 and C7 models compared with C9. This represents an increase of 6.34% and 4.39% for the collapse load.

It can be concluded that models with same dent lengths and dent depths are different with increasing dentin depth, the model is strengthened. And the depth of penetration, Dent is a booster element for the model. On the other hand, if the initial loading load and flexural failure of each model are compared to ours, the overall load bucklings compared to the initial buckling loads are 1.38, 1.24, 1.67, 1.48, and 1.40 for C6, C7, C8, C9, and the C10 models, respectively. After the initial load buckling of the models, they resisted the models themselves. They entered the stage of post buckling. A fading effect is seen in all models.

In general, it can be said that the collapse load is about 1.5 times the initial load buckling. Now, if we compare the perfect sample C10 with the other test models according to Table 4.1, for C10’s initial buckling load and models C6–C9, we can say that increased by

31.95, 25.85, 18.47, and 11.04%, respectively, the overall buckling increased by 32.61, 34.23, 2.69, and 6.33%, respectively. The collapse buckling load increased by 30.31, 30.81, 25.58, and 27.63%, respectively, compared to the C6 and C7 and C8 models, C9 model.

Table 4.1. Initial buckling, overall buckling and collapse of all tests.

Group	Specimen	Initial buckling (kPa) P_1	overall buckling (kPa) P_2	Collapse buckling (kPa) P_3	Experimental wave	Approximate Waves (Fatemi *et al.* 2013; Teng *et al.* 2001)
Without CFRP	C1/h/2/t	67.54	123.06	188.32	10	13
	C2/h/3/t	88.25	119.67	214.05	8	13
	C3/h/2/2t	82.36	135.01	231.08	8	13
	C4/h/3/2t	88.92	139.28	275.61	8	13
	C5	121.66	177.40	269.64	9	13
with CFRP	C6	90.47	125.57	195.62	8	13
	C7	98.58	122.54	194.21	8	13
	C8	108.38	181.31	208.88	9	13
	C9	118.26	174.52	203.14	9	13
	C10	132.94	186.32	280.70	7	13

4.5. Comparison of Buckling Load of First and Second Groups

In comparing the with-CFRP group to the without-CFRP group, each of the models in group 1 is compared with one another in group 2. The results are listed in Table 4.2. The buckling load of group 2 increased by about 25.34% to about 8.49% than group 1. If we compare the overall buckling score of group 2 to group 1, it increased by about 20.19%–2.34%. In the case of collapse, we cannot say that owing to raising the edge cannot be commented correctly. On the other hand, since the initial buckling load is important in this type of structure, the use of CFRP at the dent sites can have a significant effect on the initial buckling load.

Table 4.2. Comparison of buckling load of first and second groups

	Present C6 to C1	Present C7 to C2	Present C8 to C3	Present C9 to C4	Present C10 to C5
Initial buckling	25.34	10.48	24.01	24.81	8.49
Overall buckling	10.48	2.34	25.54	20.19	4.79
Collapsed buckling	3.73	-10.22	-10.63	-35.67	3.94

4.6. Comparison of Theory with First and Second Groups

Table 4.3 shows the buckling load obtained from the theoretical formulas, and Table 4.4 shows a comparison of the buckling loads obtained from experiments and theory. For example, Table 4.4 shows a comparison between the initial and overall buckling values obtained from Jawad and Venstel and Krauthaer with the initial and overall buckling tests. In the case of the without-CFRP group, the initial buckling load obtained from the experiments is about 3.52–1.95 times the buckling load obtained from the Jawad and Venstel and Krauthaer theory, and the overall load is about 5.13–3.46 times, which is for the CFRP group for load

The initial buckling obtained from the experiments is about 3.84–2.61 times the buckling load obtained from the Jawad and Venstel and Krauthaer theory, while the overall buckling load is 5.39–3.54. In the case of the without-CFRP group, the initial buckling load obtained from the experiments is about 1.9–3.42 times the buckling load obtained from the Ross theory, and the overall load is about 3.36–4.99 times, which is for the CFRP group for load. The initial buckling obtained from the experiments is about 3.74–2.54 times the buckling load obtained from the Ross theory, while the overall buckling load is 3.44–5.10.

In the case of the without-CFRP group, the initial buckling load obtained from the experiments is about 2.02–3.65 times the buckling load obtained from the BSI theory, and the overall load is about 3.59–5.32 times, which is for the CFRP group for load. The

initial buckling obtained from the experiments is about 2.71–3.99 times the buckling load obtained from the BSI theory, while the overall buckling load is 3.68–5.59.

In the case of the without-CFRP group, the initial buckling load obtained from the experiments is about 1.84–3.32 times the buckling load obtained from the ECCS theory, and the overall load is about 3.27–4.85 times, which is for the CFRP group for load. The initial buckling obtained from the experiments is about 2.47–3.63 times the buckling load obtained from the ECCS theory, while the overall buckling load is 3.35–5.09.

In general, we can assume that if we take the buckling load obtained from theories without testing, the buckling load obtained from the theories is far smaller than the initial and overall buckling loads and even the collapse of the experiments. That is, if the enavotoso is built, it will not be cost effective. On the other hand, if we want to get the initial and overall buckling times according to theoretical formulas, we must multiply the coefficients to obtain the initial and overall buckling and collapse buckling.

Table 4.3. Theoretical predictions for relevant theories in section 2.6.

	Jawad P_J (kPa)	Venstel and Krauthaer P_{VK} (kPa)	Ross P_R (kPa)	BSI P_{BSI} (kPa)	ECCS P_{ECCS} (kPa)
Perfect model	34.56	34.56	35.54	33.29	36.56

Table 4.4. Comparison of the buckling loads obtained from experiments and theory

Group	specimen	P1(kPa)	P2(kPa)	P_1/P_J	P_2/P_J	P_1/P_{VK}	P_2/P_{VK}	P_1/P_{PR}	P_2/P_R	P_1/P_{BSI}	P_2/P_{BSI}	P_1/P_{ECCS}	P_2/P_{ECCS}
Without CFRP	C1	67.54	123.06	1.954282	3.560763889	1.954282	3.560764	1.900394	3.462577	2.028837	3.696606	1.847374	3.365974
	C2	88.25	119.67	2.55353	3.462673611	2.55353	3.462674	2.483118	3.367192	2.650946	3.594773	2.41384	3.273249
	C3	82.36	135.01	2.383102	3.906539352	2.383102	3.906539	2.317389	3.798818	2.474016	4.055572	2.252735	3.692834
	C4	88.92	139.28	2.572917	4.030092593	2.572917	4.030093	2.50197	3.918965	2.671072	4.183839	2.432166	3.809628
	C5	121.66	177.4	3.520255	5.133101852	3.520255	5.133102	3.423185	4.991559	3.654551	5.328928	3.327681	4.852298
with CFRP	C6	90.47	125.57	2.617766	3.633391204	2.617766	3.633391	2.545582	3.533202	2.717633	3.772004	2.474562	3.434628
	C7	98.58	122.54	2.852431	3.545717593	2.852431	3.545718	2.773776	3.447946	2.96125	3.680985	2.696389	3.351751
	C8	108.38	181.31	3.135995	5.246238426	3.135995	5.246238	3.049522	5.101576	3.255632	5.44638	2.964442	4.959245
	C9	118.26	174.52	3.421875	5.049768519	3.421875	5.049769	3.327518	4.910523	3.552418	5.242415	3.234683	4.773523
	C10	132.94	186.32	3.846644	5.391203704	3.846644	5.391204	3.740574	5.242544	3.993391	5.596876	3.636214	5.09628

4.7. Comparison of Failures in Groups

Table 4.1 shows the number of waves obtained from the experiments and the theory of Donnell. It is well seen that the number of waves obtained from the theory in group 1 is between 3 and 5 more than the number of waves obtained from the experiments. The values in group 2 are between 5 and 6. On the other hand, in the case of the C10 model, it can be said that after modeling the buckling wave in the experimental model after leaving the CFRP device, the waves returned to a relatively basic state. This means that in the fully enclosed model with CFPR, the resulting waves can be elastoplastic.

By contrast, Figure 4.40 shows the effect of the failure of the waves, the length of each wave, and the location of the dents within the waves. The failures in all of the samples are in the forms of ٧ and ٨, that is, raising the edge in the forms of ٧ and ٨causes the model to fail. In all group-1 models, the first buckling wave was observed from the locations of the dents, while in group 2, the first buckling wave was not the location of the dents.

Table 4.5 shows the magnitude of the wavelengths obtained in Fig. 4.40, which is well seen when the waves do not have the same length. While in theoretical formulas it is that waves of uniform length and size are formed. In general, we can say that the theoretical formula for calculating buckling waveforms in the non-dent mode is more than the number of waves obtained from the experiments. On the other hand, crashes are in the form of an uplifted edge in the forms of ٧ and ٨ . If a model is completely enclosed with CFRP, after the waveform experimentation and the test is stopped, the waves of the model that were clearly seen then disappear. That is, the model is in elastoplastic mode. In the case of group 2, it can be said that the waves in the dent range vary from 20 to 60 mm.

In the load-strain curves in section 4, we can say that the strain load diagram has a uniform behavior with load-displacement graphs, that is, uniform behavior indicates the correctness of the experiments. On the other hand, at the time of the creation of the first

waves of all strain load diagrams, they were in an elastic state. However, after entering the phases, the graphs entered the plastic stage.

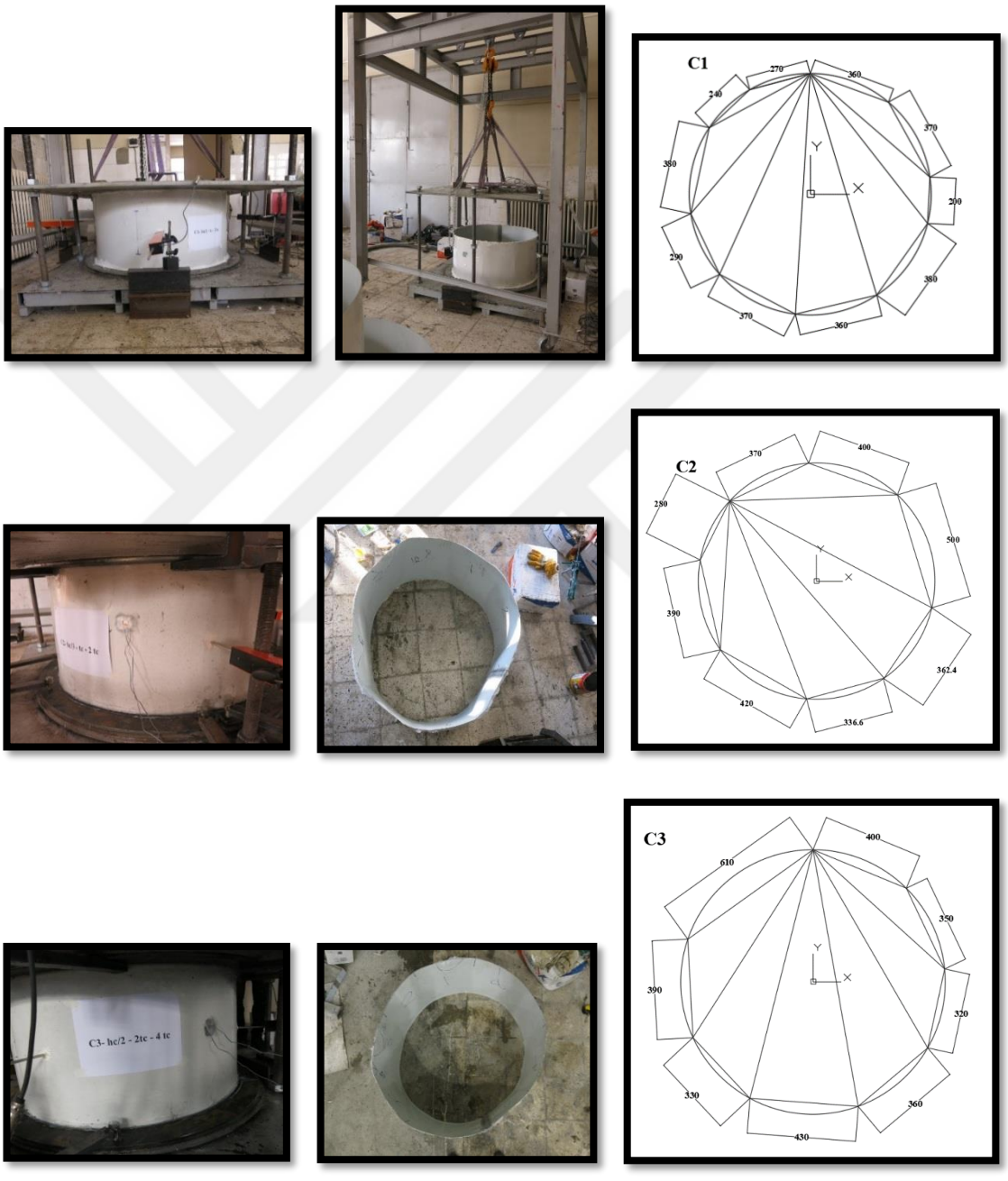

Figure 4.40. (Continued)

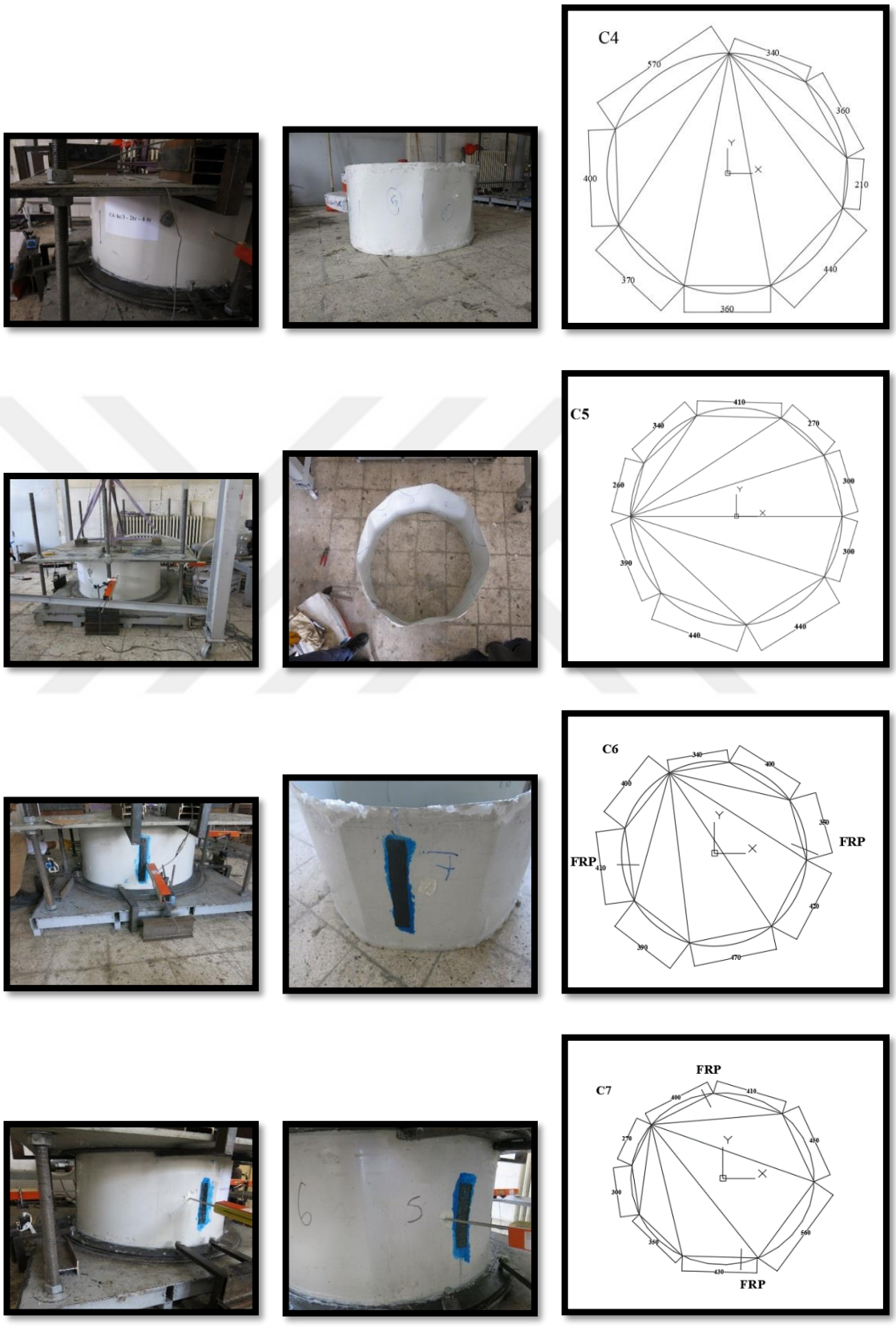

Figure 4.40. (Continued)

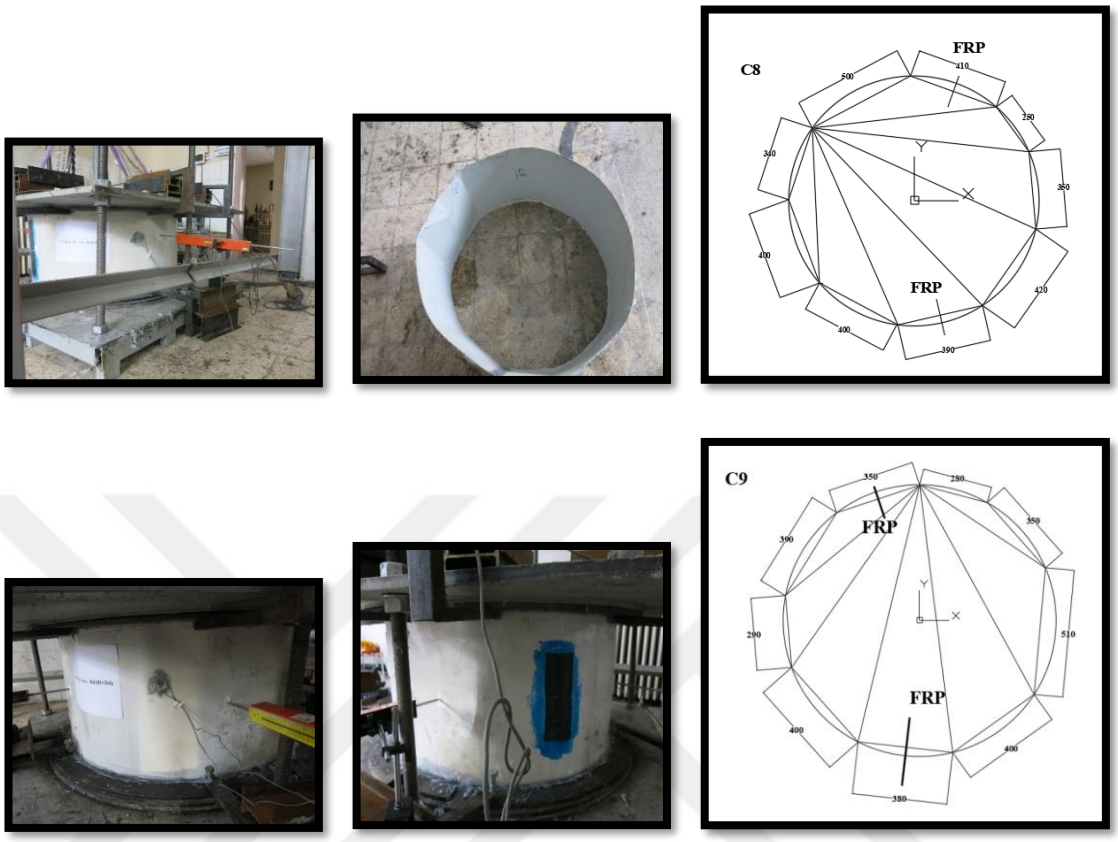

Figure 4.40. Failure of the waves, the length of each wave, and the location of the dents within the waves

Table 4.5. The magnitude of the wavelengths for all models

Group	specimen	Length of 1. Wave (mm)	Length of 2. Wave (mm)	Length of 3. Wave (mm)	Length of 4. Wave (mm)	Length of 5. Wave (mm)	Length of 6. Wave (mm)	Length of 7. Wave (mm)	Length of 8. Wave (mm)	Length of 9. Wave (mm)	Length of 10. Wave (mm)
Without CFRP	C1	360	370	200	380	360	370	290	380	240	270
	C2	370	400	500	362.4	336.6	420	360	280	-	-
	C3	400	350	320	360	430	330	390	610	-	-
	C4	340	360	210	440	360	370	400	570	-	-
	C5	260	340	410	270	300	300	440	440	390	-
with CFRP	C6	340	400	350*	420	470	390	410*	400	-	-
	C7	400*	410	450	560	430*	350	300	270	-	-
	C8	500	410*	250	350	420	390*	400	400	340	-
	C9	280	350	510	400	380*	400	290	390	350*	-

* Dent location

5. CONCLUSIONS AND RECOMMENDATIONS

In this research, we introduce dents at different depths of t_c and $2t_c$, and different lengths of h/3 and h/2, into cylindrical tanks. The models are divided into two groups: without CFRP group and with CFRP group. Each group is compared to the individual elements of the group itself, and then we compare the two groups together. We compare all initial and overall buckling and collapse by using theoretical formulas. Finally, the buckling waves (using the theory of buccaneering) and the method of reversal are described. The purpose of these studies is to investigate the effect of CFRP on dents and the effect of CFRP on dents in order to examine the buckling of the cylinder. The key findings and observations are presented as follows:

- Without CFRP group: In this group, the buckling load decreases with increasing amplitude at the same depth of penetration. It can be concluded that models with same dent lengths and dent depths are different with increasing dent depths, and the model is strengthened. And the depth of penetration, Dent is a booster element for the model. On the other hand, if the initial loading load and flexural failure of each model are compared to tested ones, the overall load buckling compared to the initial buckling load of 2.78, 2.45, 2.81, 3.1, and 2.22 for the C1, C2, C3, C4, and C5 models, respectively. After the initial load buckling of the models, they resisted the models themselves. They entered the stage of post buckling. A fading effect is seen in all models. In general, the collapse load is about 2.5 times the initial load buckling.
- With CFRP group: the buckling load decreased with increasing amplitude at the same depth of penetration. It can be concluded that models with same dent lengths and dent depths are different with increasing dentin depth, the model is strengthened. And the depth of penetration, Dent is a booster element for the model. On the other hand, if the initial loading load and flexural failure of each model are compared to ours, the overall load bucklings compared to the initial buckling loads are 1.38, 1.24, 1.67, 1.48, and 1.40 for C6, C7, C8, C9, and the C10 models, respectively. After the initial load buckling of the models, they resisted the models themselves. They entered the stage of post buckling.

A fading effect is seen in all models. In general, it can be said that the collapse load is about 1.5 times the initial load buckling.

- Comparison of buckling load of without CFRP group with and CFRP group: The buckling load of CFRP group increased by about 25.34% to about 8.49% than without CFRP group. If we compare the overall buckling score of CFRP group to without CFRP group, it increased by about 20.19%–2.34%. In the case of collapse, we cannot say that owing to raising the edge cannot be commented correctly. On the other hand, since the initial buckling load is important in this type of structure, the use of CFRP at the dent sites can have a significant effect on the initial buckling load.
- Comparison of theory with groups: In general, we can assume that if we take the buckling load obtained from theories without testing, the buckling load obtained from the theories is far smaller than the initial and overall buckling loads and even the collapse of the experiments. On the other hand, if we want to get the initial and overall buckling times according to theoretical formulas, we must multiply the coefficients to obtain the initial and overall buckling and collapse buckling.
- Comparison of failures in groups: The failures in all of the samples are in the forms of ۷ and ۸, that is, raising the edge in the forms of ۷ and ۸causes the model to fail. In all without CFRP-group models, the first buckling wave was observed from the locations of the dents, while in CFRP-group, the first buckling wave was not the location of the dents. We can say that the theoretical formula for calculating buckling waveforms in the non-dent mode is more than the number of waves obtained from the experiments. On the other hand, crashes are in the form of an uplifted edge in the forms of ۷ and ۸. If a model is completely enclosed with CFRP, after the waveform experimentation and the test is stopped, the waves of the model that were clearly seen then disappear. That is, the model is in elastoplastic mode. In the case of CFRP-group, it can be said that the waves in the dent range vary from 20 to 60 mm. In the load-strain curves, we can say that the strain load diagram has a uniform behavior with load-displacement graphs, that is, uniform behavior indicates the correctness of the experiments. On the other hand, at the time of the creation of the first waves of all strain load diagrams, they were in an elastic state. However, after entering the phases, the graphs entered the plastic stage.

Throughout the experimental test the verify dents and dimensions of CFRP are decided as constant. However, experimental observations have to be realized for varying geometries and dimensions of CFRP. Furthermore, CFRP product type, material properties are the other concerns.

From the point of stability of thin-walled shells; the thickness and thickness variation of shells, thickness optimization, size effect etc. are the should done studies for the future works.

REFERENCE

Aghajari S, Abedi K, Showkati H. Buckling and post-buckling behavior of thin-walled cylindrical steel shells with varying thickness subjected to uniform external pressure. Thin Walled Struct 2006;44:904–9.

Aydın, A.C., Kılıç, M., Maali, M. and Sagiroglu, M., "Experimental Assessment of the Semi-Rigid Connections Behavior with Angles and Stiffeners", Journal of Constructional Steel Research, 114, November 2015, 338-348.

Aydın, A.C., Maali, M., Kılıç, M. and Sagiroglu, M., "Experimental Investigation of Sinus Beams with End-Plate Connections", Thin-Walled Structures, 97, December 2015, 35-43.

Batikha, M.x J.F.Chen, J.M.Rotter, J.G.Teng. Strengthening metallic cylindrical shells against elephant's foot buckling with FRP. Thin-Walled Structures 47(2009)1078–1091.

Brush, D.O., Almorth, B.O. (1975). "Buckling of Bares, Plates and Shells", Mc Grow Hill, New York.

BSI, 2000. Specification for unfired fusion welded pressure vessels. BSI; 2000.

BSI, 2009. Specification for Unfired Fusion Welded Pressure Vessels, 4th ed. British Standards Institution, UK PD5500.

Chen, W.F, Lui , E.M. (1987)."Structural Stability", Elsevier.

DIN 18800. Stahlbauten. Teil 4: Stabilitätsfalle, Schalenbeulen; 1990.

ECCS EDR5. European recommendations for steel construction. Buckling of shells. In: Rotter JM, Schmidt H, editors. 5th ed. Brussels: European convention for constructional steelwork; 2008 [384 pp.].

ECCS, 1988. Buckling of Steel Shells – European Recoendations, Belgium. ECCSCECM-EKS, European Convention for Constructional Steelwork.

ENV 1993-1-6: Eurocode 3Design of steel structures, Part 1.6: general rules—strength and stability of shell structures. Eurocode 3 Part 1.6. Brussels: CEN; 2007.

European Convention for Constructional Steelwork (ECCS). Buckling of steel shells—European recommendations. Belgium: ECCS-CECM-EKS; 1988.

Farshad , M. (1994). "Stability of Structures". 2nd ed., Mc Grow Hill, New York .

Fatemi SM, Showkati H, Maali M. Experiments on imperfect cylindrical shells under uniform external pressure. Thin Walled Struct 2013;65:14–25.

Ghanbari Ghazijahani T, Jiao H, Holloway D. Experimental study on damaged cylindrical shells under compression. Thin Walled Struct 2014;80:13–21.

Ghanbari Ghazijahani T, Showkati H. Experiments on cylindrical shells under pure bending and external pressure. J Constr Steel Res 2013;88:109–22.

Ghanbari Ghazijahani T, Zirakian T. Determination of buckling loads of conical shells using extrapolation techniques. Thin Walled Struct 2014;74:292–9.

Ghazijahani TG, Jiao H, Holloway D. An experimental study on externally pressurized stiffened and thickened cylindrical shells. Thin Walled Struct 2014;85:359–66.

Ghazijahani TG, Jiao H, Holloway D. An experimental study on externally pressurized stiffened and thickened cylindrical shells. Thin-Walled Structures 85(2014c)359–366.

Ghazijahani TG, Jiao H, Holloway D. Experimental study on damaged cylindrical shells under compression. Thin-Walled Structures 80(2014a)13–21.

Ghazijahani TG, Jiao H, Holloway D. Experiments on dented cylindrical shells under peripheral pressure. Thin Walled Struct 2014;84:50–8.

Ghazijahani TG, Jiao H, Holloway D. Experiments on dented cylindrical shells under peripheral pressure. Thin-Walled Structures 84(2014b)50–58.

Ghazijahani TG, Jiao H, Holloway D. Fatigue experiments on circular hollow sections with CFRP reinforced cutouts. Journal of Constructional Steel Research 106 (2015a) 322–328.

Ghazijahani TG, Jiao H, Holloway D. Longitudinally stiffened corrugated cylindrical shells under uniform external pressure. Journal of Constructional Steel Research 110 (2015b) 191–199

Ghazijahani TG, Jiao H, Holloway D. Plastic buckling of dented steel circular tubes under axial compression: An experimental study. Thin-Walled Structures 92(2015c) 48–54.

Ghazijahani TG, Jiao H, Holloway D. Timber filled CFRP jacketed circular steel tubes under axial compression. Construction and Building Materials 94 (2015d) 791–799.

Ghazijahani TG, Jiao H, Holloway D., Longitudinally stiffened corrugated cylindrical shells under uniform external pressure, Journal of Constructional Steel Research 110 (2015) 191–199

Ghazijahani TG, Showkati H. Experiments on conical shell reducers under uniform external pressure. J Constr Steel Res 2011;67:1506–15.

Ghazijahani TG, Showkati H. Locally imperfect conical shells under uniformexternal pressure. Strength Mater 2013;45:369–77.

Golzan B, Showkati H. Buckling of thin-walled conical shells under uniform external pressure. Thin Walled Struct 2008;46:516–29.

Jawad MH. Theory and design of plate and shell structures. Chapman & Hall; 1994.

Love, A.E.H. (1959). “A treatise on the mathematical theory of elasticity”, 4th ed., Dover Publisher , New York.

Maali M, Showkati H, Mahdi Fatemi S. Investigation of the buckling behavior of conical shells under weld-induced imperfections. Thin Walled Struct 2012;57:13–24.

Maali, M., Aydin, A.C. and Sagiroglu, M., "Investigation of innovative steel runway beam in industrial building", Microsilica SADHANA Academy Proceedings in Engineering Sciences, 40, October 2015, 2239-2251.

Maali, M., Kılıç, M. and Aydın, A.C., "Experimental Model of the Behaviour of Bolted Angles Connections with Stiffeners", Int. Journal of Steel Structures, 16(3):1-15, 2016.

Maali, M., Kılıç, M., Sagiroglu, M. and Aydın, A.C., "Experimental Model for Predicting the Semi-Rigid Connections’ Behaviour with Angles and Stiffeners", Advances in Structural Engineering, 2017, 20(6), 884-895.

Mahdi. E ., Hamouda, A, M., Sahari, B. B., and Khalid, Y. A., (2002) , “Crushing Behavior of Cone-Cylinder-Cone Composite System,” Mech. Adv. Mater. Structures, 9(2), pp, 99-117.

Mazurkiewicz , Z.E., Nagorski, R.T. (1991). “Shells of Revolutions”, Elsevier.

Miller, C.D (1999). Shell Structure. CRC press LIC.

Niloufari A, Showkati H,MaaliM, Mahdi Fatemi S. Experimental investigation on the effect of geometric imperfections on the buckling and post-buckling behavior of steel tanks under hydrostatic pressure. Thin Walled Struct 2014; 74:59–69.

Ross CT. A proposed design chart to predict the inelastic buckling pressures for conical shells under uniform external pressure. Mar Technol 2007;44:77–81.

Ross, C.T.F., 2007. A proposed design chart to predict the inelastic buckling pressures for conical shells under uniform external pressure. Mar. Technol. 44 (2), 77–81.

Sagiroglu, M., Experimental evaluation of the post-fire behavior of steel T-component in the beam-to-column connection, Fire Safety Journal, Vol: 96, pp.153-164, 2018.

Sagiroglu, M., Maali, M., Kılıç, M. and Aydın, A.C., A Novel Approach for Bolted T-Stub Connections, International Journal of Steel Structures, 2018, Vol:18, Issue:2, pp. 420-426.

Showkati , H, Ansourian , P,.(1995)"Influence of primary boundary conditions on the buckling of Shallow cylindrical shells" Constructional steel Research,Vol.36,No. 1. pp. 53-75.

Showkati H, Ansourian P. Influence of primary boundary conditions on the bucklingof shallow cylindrical shells. J Constr Steel Res 1996;36:53–75.

Showkati H, Shahandeh R. Experiments on the buckling behavior of ring-stiffened pipelines under hydrostatic pressure. J Eng Mech 2009;136:464–71.

Teng JG, Zhao Y, Lam L. Techniques for buckling experiments on steel silo transition junction. Thin-Walled Structures ,2001;39:685–707.

Teng JG, Zhao Y, Lam L. Techniques for buckling experiments on steel silo transition junction. Thin-Walled Structures ,2001;39:685–707.

Teng, J.G. Y.M. Hu. Behaviour of FRP-jacketed circular steel tubes and cylindrical shells under axial compression. Construction and Building Materials 21 (2007) 827–838.

Timoshenko, S.P., Gere, I.M. (1961). "Theory of Elastic Stability", 2th ed., Mc Grow Hill, New York.

Vakili M, and Showkati H,. Experimental and Numerical Investigation of Elephant Foot Buckling and Retrofitting of Cylindrical Shells by FRP. Journal of Composites for Construction. 2015. DOI: 10.1061/(ASCE)CC.1943-5614.0000640.

Venstel, E., Krauthaer, T., 2001. Thin Plates and Shells: Theory: Analysis, and Applications. Marcel Dekker, Inc., New York.

RESUME

Ali AGHAZADEH DIZAJI was born in Azarshahr, in 1981. He received his bachelor degree in civil engineering from Azad University, department of Civil Engineering, Tabriz İran. He had been working in various construction projects as civil engineer. He began his master degree in Atatürk University in 2014 and he is deputy manager of Razi. Company, Tabriz, Iran.